

Formation of Disk Galaxies: Warm Dark Matter and the Angular Momentum problem

Jesper Sommer-Larsen and Alexandre Dolgov

Theoretical Astrophysics Center, Juliane Maries Vej 30, DK-2100 Copenhagen Ø, Denmark

ABSTRACT

We have performed TREESPH simulations of disk galaxy formation in various warm dark matter (WDM) cosmologies. Our results indicate that for a range of WDM free-streaming masses, the disk galaxy formation angular momentum problem can be considerably alleviated (and we speculate: perhaps even completely resolved) by going to the WDM structure formation scenario, without having to invoke stellar feedback processes. They also strongly suggest that part of the angular momentum problem is due to numerical effects, most likely related to the shock capturing, artificial viscosity used in SPH. Furthermore we find that we can match the observed *I*-band Tully-Fisher (TF) relation, provided that the mass-to-light ratio of disk galaxies is $(M/L_I) \simeq 0.6\text{--}0.7$. We argue that this is a fairly reasonable value in comparison with various dynamical and spectrophotometric estimates, including two given in this paper. Finally, we discuss possible physical candidates for WDM particles extensively. We find that the most promising are neutrinos with weaker or stronger interactions than normal, majorons (light pseudogoldstone bosons) or mirror or shadow world neutrinos.

Subject headings: cosmology: theory — dark matter — galaxies: formation — galaxies: structure — elementary particles — methods: numerical

1. Introduction

The formation of galactic disks is one of the most important unsolved problems in astrophysics today. In the currently favored hierarchical clustering framework, disks form in the potential wells of dark matter halos as the baryonic material cools and collapses dissipatively. It has been shown (Fall & Efstathiou 1980) that disks formed in this way can be expected to possess the observed amount of angular momentum (and therefore the

observed spatial extent for a given mass and profile shape), but only under the condition that the infalling gas retain most of its original angular momentum.

Numerical simulations of this collapse scenario in the cold dark matter cosmological context (e.g., Navarro & Benz 1991, Navarro & White 1994, Navarro, Frenk, & White 1995), however, have so far consistently indicated that when only cooling processes are included the infalling gas loses too much angular momentum (by over an order of magnitude) and the resulting disks are accordingly much smaller than required by the observations. This discrepancy is known as the *angular momentum problem* of disk galaxy formation. It arises from the combination of the following two facts: a) In the CDM scenario the magnitude of linear density fluctuations $\sigma(M) = <(\delta M/M)^2>^{1/2}$ increases steadily with decreasing mass scale M leading to the formation of non-linear, virialized structures at increasingly early epochs with decreasing mass i.e. the hierarchical “bottom-up” scenario. b) Gas cooling is very efficient at early times due to gas densities being generally higher at high redshift as well as the rate of inverse Compton cooling also increasing very rapidly with redshift ($\propto (1+z)^4$). a) and b) together lead to rapid condensation of small, dense gas clouds, which subsequently lose energy and (orbital) angular momentum by dynamical friction against the surrounding dark matter halo before they eventually merge to form the central disk. A mechanism is therefore needed that prevents, or at least delays, the collapse of small protogalactic gas clouds and allows the gas to preserve a larger fraction of its angular momentum as it settles into the disk. (Such a mechanism is also helpful in solving the *overcooling problem*, namely the observation (White & Rees 1978) that cooling is expected to be so efficient at early times that most of the gas should have been converted to stars well before the assembly of present-day galactic disks). Weil, Eke, & Efstathiou (1998) have shown that if the early cooling is suppressed (by whatever means), numerical simulations can indeed yield more realistically sized disks - see also Eke, Efstathiou & Wright (1999). The physical mechanism by which cooling is suppressed or counteracted, however, was not specified.

Sommer-Larsen et al. (1999, hereafter SLGV99) discussed the effects of various stellar reheating mechanisms in more detail using numerical TREESPH simulations of disk galaxy formation in a CDM cosmological context. They found that more or less uniform reheating of the Universe resulting from a putative early epoch of population III star formation ($z \gtrsim 6$) does not lead to a solution to the angular momentum problem, but that localized star-bursts in protogalactic gas clouds might: *If* the star-bursts can blow the remaining, bulk part of the gas out of the small and dense dark matter halos of the clouds, then the test simulations of SLGV99 show that the gas later gradually settles forming an extended, high angular momentum disk galaxy in the central parts of a large, common dark matter halo. The physics of global gas blow-out processes were considered in early calculations by Dekel

& Silk (1986) and Yoshii & Arimoto (1987) indicating that star-bursts might well blow out most of the gas in small galaxies with characteristic circular speed (where the rotation curve is approximately constant) $V_c \lesssim 100$ km/s. Unfortunately, more recent, detailed simulations by Mac Low & Ferrara (1999) suggest that this global blow-out scenario may not work so well, even in small (disk) galaxies: The star-bursts typically lead to bipolar outflows of very hot gas perpendicular to the disk of the small galaxy, only expelling a minor fraction of the disk gas.

Moreover, various possible shortcomings of the CDM cosmological scenario in relation to structure formation on galactic scales have recently been discussed in the literature: 1) CDM possibly leads to the formation of too many small galaxies relative to what is observed, i.e. the *missing satellites problem* (e.g., Klypin et al. 1999). 2) Even if galactic winds due to star-bursts can significantly reduce the number of visible dwarf galaxies formed, sufficiently many of the small and tightly bound dark matter systems left behind can still survive to the present day in the dark matter halos of larger galaxies like the Milky Way to possibly destroy the large, central disks via gravitational heating, as discussed by Moore et al. 1999a. 3) The dark matter halos produced in CDM cosmological simulations tend to have central cusps with $\rho_{DM}(r) \propto r^{-N}$, $N \sim 1 - 2$ (Dubinski & Carlberg 1991, Navarro et al. 1996, Fukushige & Makino 1997, Moore et al. 1998, Kravtsov et al. 1998, Gelato & Sommer-Larsen 1999). This is in disagreement with the flat, central dark matter density profiles (cores) inferred from observations of the kinematics of dwarf and low surface brightness galaxies (e.g., Burkert 1995, de Blok & McGaugh 1997, Kravtsov et al. 1998, Moore et al. 1999b, but see also van den Bosch et al. 1999).

The first two problems may possibly be overcome by invoking warm dark matter (WDM) instead of CDM: WDM is similar to CDM on mass scales larger than the free-streaming mass $M_{f,WDM} \sim 10^{10}\text{-}10^{12} M_\odot$, but density fluctuations $\sigma_{WDM}(M)$ are suppressed on mass scales $M < M_{f,WDM}$ relative to CDM (but note that they are still non-zero as $\sigma_{WDM}(M < M_{f,WDM}) \simeq \sigma_{WDM}(M_{f,WDM})$ - see section 2). As a consequence, fewer low mass galaxies (or “satellites”) are formed cf., e.g., Moore et al. (1999a) and section 2 of this paper. The central cusps problem may be more generic cf. Huss et al. (1999) and Moore et al. (1999b), but the WDM scenario deserves further attention also on this point. In particular the fact the momentum part of the phase-space distribution function is not approximately singular at redshifts where all perturbations are still in the linear regime, but has a finite width (or equivalently: velocity dispersion) due to free-streaming may be very helpful in solving the central cusps problem, as recently discussed by Hogan (1999) - see also Hogan & Dalcanton (2000), Dalcanton & Hogan (2000) and Madsen (2000).

In this paper we show that the disk galaxy formation angular momentum problem can

be considerably alleviated by invoking the WDM rather than the CDM structure formation scenario and this without having to appeal to stellar feedback processes. The main reason for this is that the inflow of gas onto the forming disk is more smooth and coherent for WDM than for CDM, resulting in considerably larger disk angular momenta, as discussed by SLGV99.

In section 2 WDM and its relation to galaxy formation is briefly discussed. Section 3 gives a short presentation of the numerical code and the initial conditions. The simulations themselves are described in section 4, and the results are analyzed in section 5. In section 6 we discuss possible physical candidates for WDM particles extensively and in section 7 we present a final discussion and summarize our conclusions.

2. Warm Dark Matter

The terms “warm” and “cold” dark matter were probably first used in Primack & Blumenthal (1983) and the implications for structure formation theory first worked out by Blumenthal et al. (1982). In this section we give a brief introduction to “conventional” warm dark matter following the approach of Bardeen et al. (1986) and using expressions from that work - see also, e.g., Primack (1981), Pagels & Primack (1982) and Pierpaoli et al. (1998). We defer a much more detailed and general discussion of the relevant particle physics to section 6.

At low redshift warm dark matter particles behave in many respects in the same way as cold dark matter (see below), but from a particle physics point of view they are quite different, however: CDM particles (apart from axions) are thought to be very massive, normally with $m \gtrsim 1$ GeV, and to be non-relativistic when they decouple from the rest of the particles in the Universe at high redshift. WDM is particles with typical masses $m \sim 1$ keV, which in conventional theory decouple at high redshifts $z_{dec} \gtrsim 10^{13}$ (or $T_{dec} \gtrsim 1$ GeV) being still ultra-relativistic. At $z_{nr} \sim 10^6$ - 10^7 the WDM particles become non-relativistic: $3kT_{WDM} \simeq m_{WDM}c^2$. The Universe is still radiation dominated at this stage, as $z_{nr} \gg z_{eq} \sim 10^4$, where z_{eq} is the redshift of matter-radiation equivalence. The horizon mass of WDM at z_{nr} defines a characteristic mass scale called the free-streaming mass $M_{f,WDM} \sim M_{H,WDM}(z_{nr})$. Perturbations on mass scales $M \lesssim M_{f,WDM}$ are damped relative to CDM due to relativistic free-streaming of the WDM particles at $z > z_{nr}$. On larger mass scales $M \gtrsim M_{f,WDM}$ WDM behaves like CDM.

Following Bardeen et al. (1986) the power spectrum of WDM (adiabatic fluctuations)

can be expressed as

$$P_{WDM}(k) = T_{WDM}^2(k) P_{CDM}(k) , \quad (1)$$

where the CDM to WDM “transfer function” can be approximated well by

$$T_{WDM}(k) = \exp \left[-\frac{kR_{f,WDM}}{2} - \frac{(kR_{f,WDM})^2}{2} \right] \quad (2)$$

and $P_{CDM}(k)$ is the CDM power spectrum for which we use the standard SCDM form. The function T_{WDM}^2 is shown in Figure 1. The comoving, free-streaming scale $R_{f,WDM}$ is given by

$$R_{f,WDM} = 0.2 \left(\frac{g_{WDM,dec}}{100} \right)^{-4/3} (\Omega_{WDM} h^2)^{-1} \text{ Mpc} , \quad (3)$$

$g_{WDM,dec}$ being the effective number of particle degrees of freedom when the WDM particles decouple. $\Omega_{WDM} h^2$ is related to the mass of the WDM particles by

$$\Omega_{WDM} h^2 = 1.0 \left(\frac{g_{WDM,dec}}{100} \right)^{-1} \left(\frac{m_{WDM}}{\text{keV}} \right) \quad (4)$$

For justification of equations (3) and (4), see section 6.

A characteristic free-streaming wave number $k_{f,WDM}$ can be defined as the k for which $T_{WDM}^2=0.5$. From Figure 1 it then follows that $k_{f,WDM} \times R_{f,WDM} \simeq 0.46$, so we define $k_{f,WDM} \equiv R_{f,WDM}/0.46$. Using this we can then define a characteristic free-streaming mass in terms of $\lambda_{f,WDM} \equiv 2\pi/k_{f,WDM}$ by

$$M_{f,WDM} \equiv \frac{4\pi}{3} \rho_{crit} \Omega_{WDM} \left(\frac{\lambda_{f,WDM}}{2} \right)^3 = 3.7 \cdot 10^{11} h^{-1} \Omega_{WDM} \left(\frac{R_{f,WDM}}{0.1 h^{-1} \text{Mpc}} \right)^3 \text{ M}_\odot \quad (5)$$

Using equations (3)-(5) we can finally express the WDM particle mass in terms of this free-streaming mass

$$m_{WDM} = 2.4 h^{5/4} \Omega_{WDM}^{1/2} \left(\frac{M_{f,WDM}}{10^{11} h^{-1} \text{M}_\odot} \right)^{-1/4} \text{ keV} . \quad (6)$$

The average relative mass fluctuations on mass scale M , $\sigma(M)$, can be calculated from the power spectrum $P(k)$ in linear theory as

$$\sigma^2(M) = \left\langle \left(\frac{\delta M}{M} \right)^2 \right\rangle = \frac{1}{(2\pi)^3} \int d^3k P(k) W(kx) , \quad (7)$$

where the weight function

$$W(y) = \frac{9}{y^6} [\sin y - y \cos y]^2 , \quad y = kx \quad (8)$$

is the square of the Fourier transform of a spherical top-hat filter of radius x (following Peebles 1980). To illustrate the difference between CDM and WDM we show in Figure 2 $\sigma(M; z = 0)$ for CDM as well as WDM with $R_{f,WDM} = 0.037, 0.075$ and $0.15 h^{-1}\text{Mpc}$ corresponding to free-streaming masses of $1.9 \times 10^{10}, 1.5 \times 10^{11}$ and $1.2 \times 10^{12} h^{-1}\text{M}_\odot$. The curves have been normalized such that $\sigma_8 = 0.5$, where σ_8 is the present day value of $\sigma(M)$ defined above for M equal to the average mass within spheres of comoving radius $8h^{-1} \text{ Mpc}$.

The fact that the $\sigma(M; z = 0)$ curves flatten at low masses for WDM does *not* mean that no low mass galaxies are formed (see also Schaeffer & Silk 1988). To illustrate this we calculate the present day ($z = 0$) mass spectrum using (linear) Press-Schechter (PS) theory: The mass spectrum $dN(M)/dM$ in the linear PS approximation is given by (e.g. White 1993)

$$\frac{dN(M)}{dM}(z = 0) = -\sqrt{\frac{2}{\pi}} \frac{\bar{\rho}}{M} \frac{\delta_c}{\sigma^2(M; z = 0)} \frac{d\sigma(M; z = 0)}{dM} \exp\left[\frac{-\delta_c^2}{2\sigma^2(M; z = 0)}\right] , \quad (9)$$

where we take $\delta_c = 1.69$ (see White 1993). The mass spectra obtained in this way for CDM and the WDM described above are shown in Figure 3. Clearly, for WDM dN/dM still decreases with M as for CDM, but, for example, for masses three orders of magnitude below the free-streaming mass dN/dM is down by more than an order of magnitude relative to CDM, whereas for masses of the order of or larger than the free-streaming mass dN/dM is essentially the same for WDM and CDM. We caution, however, that the PS theory applied above is not completely rigorous and hence that N-body WDM simulations should be undertaken to determine WDM mass spectra more properly.

3. The code and the initial conditions

3.1. The code

We use the gridless Lagrangian N -body and Smoothed Particle Hydrodynamics code TREESPH described in SLGV99. Our TREESPH code is modeled after that of Hernquist & Katz (1989).

We include gas cooling and heating terms as in Vedel et al. (1994). The heating corresponds to a redshift-dependent, homogeneous and isotropic UVX background field. We assume a rather hard (spectral index -1) quasar like field

$$J_\nu(z) = J_{-21}(z) \times 10^{-21} \left(\frac{\nu}{\nu_L}\right)^{-1} \text{ erg cm}^{-2} \text{ sr}^{-1} \text{ Hz}^{-1} \text{ s}^{-1}, \quad (10)$$

where ν_L is the Lyman limit frequency, with the redshift-dependent normalization

$$J_{-21}(z) = \frac{10}{1 + [5/(1+z)]^4} \quad (11)$$

of Efstathiou (1992). For greater realism one could build on the detailed study of Haardt & Madau (1996), but our adopted background field is quantitatively not too dissimilar from theirs (once allowance is made for our simplified spectral shape), at least at redshifts $z \lesssim 3$, and should be adequate for the level of detail we can represent in the simulations. The code furthermore incorporates inverse Compton cooling, which is also explicitly redshift-dependent.

SLGV99 studied the effects of star-formation in terms of the subsequent energy and momentum feedback processes to the gas as a means of resolving the angular momentum problem of disk galaxy formation. In this paper we study the effects of going from CDM to WDM, as an alternative. In order to separate the various effects clearly we describe in this paper what in SLGV99 was dubbed “passive” simulations, i.e. simulations with no star-formation and feedback effects.

The smoothing length of each SPH particle is adjusted so as to keep the number of neighbors close to 50.

3.2. The initial conditions

Our cosmological initial conditions are based on a standard ($\Omega_M = 1$, $\Omega_\Lambda = 0$) CDM model with Hubble constant $H_0 = 100h \text{ km s}^{-1} \text{ Mpc}^{-1} = 50 \text{ km s}^{-1} \text{ Mpc}^{-1}$. On the scales of interest to us the effective index of the power spectrum is approximately -2 ($P(k) \propto k^{-2}$). Following Eke, Cole, & Frenk (1996) we normalize the spectrum to $\sigma_8(z=0) = 0.5$, where as customary σ_8^2 is the mass variance within spheres of comoving radius $8h^{-1} \text{ Mpc}$, extrapolated from the linear regime of perturbation growth. We note that a σ_8 of 0.5 is somewhat lower than the value of 0.67 usually used in what is called “standard CDM”.

We begin by performing a large-scale simulation within a sphere of comoving radius 40 Mpc. Individual halos are then selected from the final state and sampled at higher resolution. The original large-scale simulation is used to provide a tidal field acting on the resampled halos, which are evolved separately in a second round of simulations.

Approximately 2.5×10^5 particles are initially placed on a cubic lattice within the large sphere. Position and velocity perturbations are then applied according to the Zel'dovich (1970) approximation. The perturbations consist of the superposition of $N_k \sim 4 \times 10^4$

plane waves sampling a Gaussian random field with variance given by the power spectrum. Following Navarro & White (1994) we use an equal number of waves per logarithmic interval in k -space. The phases of these waves are random and only wavenumbers between the fundamental and Nyquist wavenumber of the lattice are included. The initial redshift (which determines the amplitude of the initial perturbations) is $z_i \simeq 18$.

The evolution of this system to $z = 0$ is then computed using a tree code. Only gravitational forces are included in this first simulation. In the final state we identify four virialized, isolated halos with circular velocities between 200 and 260 km s^{-1} in the innermost 20 Mpc of the simulation. We expect that a significant fraction of such halos should host disk galaxies similar to the Milky Way since the circular velocities are in the same range and our halos were chosen to lie “in the field”, away from larger concentrations of mass. We adopt the customary working definition of the virial radius as the radius r_{200} of a sphere enclosing a mean density of 200 times the critical cosmic value. Tracing the particles in these halos back to the initial conditions, we find that they all come from regions that fit within spheres of comoving radius ~ 3 Mpc.

Each of these spheres at $z \simeq 18$ is then resampled with a lattice 4 times finer in each spatial dimension in our moderate resolution (MR) simulations and 8 times finer in our high resolution (HR) simulations. Each sphere contains about 7000 points of this new lattice in our MR simulations and about 56000 points in our HR simulations. We assign one dark matter (DM) particle and two SPH particles to each of these points for the MR simulations and one DM particle and one SPH particle to each point for the HR simulations. The SPH particles are positioned at random within one gas gravitational softening length (see below) of their parent DM particle. Note that at this redshift the DM particles are spaced by about 14 kpc for the MR simulations and 7 kpc for the HR simulations, so that each SPH particle is rather closely associated with its parent DM particle. Table 1 lists the precise number of SPH and DM particles in each sphere. We generally use a baryonic mass fraction $\Omega_b = 0.05$, consistent with nucleosynthesis constraints ($0.01h^{-2} \lesssim \Omega_b \lesssim 0.02h^{-2}$), but use $\Omega_b = 0.10$, which is more consistent with the observationally determined baryonic fractions in galaxy groups and clusters, in some of the MR simulations. This leads to masses of $1.1 \times 10^9 M_\odot$ for the DM and $2.9 \times 10^7 M_\odot$ for the SPH particles for the MR simulations with $\Omega_b = 0.05$, 1.0×10^9 and $5.8 \times 10^7 M_\odot$ respectively for the $\Omega_b = 0.10$ MR simulations and 1.4×10^8 and $7.3 \times 10^6 M_\odot$ for the HR simulations, which all have $\Omega_b = 0.05$. The SPH particles are assigned an initial thermal energy corresponding to a temperature $T_i \simeq 100$ K. In order to include small-scale power that could not be sampled in the first simulation, we add shorter-wavelength plane waves in a way that preserves an equal number of waves per interval in $\log k$. Given the variety of properties of the WDM particle candidates discussed in section 6 and that the purpose of this paper is to investigate qualitatively the effects on

disk galaxy formation of going from CDM to WDM we approximate $T_{WDM}(k)$ by a step function

$$\tilde{T}_{WDM}(k) = \begin{cases} 1 & k \leq k_c, \\ 0 & k > k_c. \end{cases} \quad (12)$$

We find that for a given $R_{f,WDM}$, $\tilde{T}_{WDM}(k)$, with $k_c = 0.46R_{f,WDM}^{-1}$ (cf. section 2), gives a reasonable match to $T_{WDM}(k)$ as shown in Figure 1 (dotted line). In Figure 2 we show by the thin solid line $\tilde{\sigma}(M; z = 0)$ for $k_c = 6.2 h \text{ Mpc}^{-1}$ (corresponding to $R_{f,WDM} \simeq 0.075 h^{-1}\text{Mpc}$). As can be seen from the figure, the match to $\sigma(M; z = 0)$ for $R_{f,WDM} = 0.075 h^{-1}\text{Mpc}$ is also reasonably good. The WDM simulations described in this paper are hence performed using the original, standard CDM power spectrum used in SLGV99, modified to WDM by

$$\tilde{T}_{WDM}(k) = \begin{cases} 1 & kR_{f,WDM} \leq 0.46, \\ 0 & kR_{f,WDM} > 0.46. \end{cases} \quad (13)$$

In this spirit we are also able to reuse the original, background CDM cosmological simulation for the WDM simulations presented in this work, as the typical WDM wavenumbers k_c used here are comparable to the Nyquist wavenumber of the CDM cosmological simulation.

We use stored intermediate results from the large cosmological simulation to provide a time-dependent tidal field acting on the resampled spheres. This is achieved by treating the original particles outside the resampled sphere as passive, interpolating their positions between successive snapshots of the original simulation and incorporating them into the particle tree that the code constructs on each step for the evaluation of gravitational forces. Gravitational interactions between particles are softened according to the prescription of Hernquist & Katz (1989), with softening lengths of 3 kpc for the gas particles and 10 kpc for the dark matter particles in the MR simulations, 1.5 and 5 kpc, respectively, in the HR simulations, and 40 kpc for the “passive” dark matter particles that provide the tidal field from the original large-scale simulation. The gravitational softening lengths are kept constant in physical units throughout the evolution of the system.

4. The simulations

For the WDM galaxy formation simulations we identify the four resampling spheres S1-S4, also used by SLGV99 for their CDM galaxy formation simulations.

It seems reasonable to assume that $M_{f,WDM} \gtrsim 10^9 - 10^{10} M_\odot$ in order for a change from CDM to WDM to have a significant impact on the disk galaxy formation angular momentum problem as well as the other possible CDM problems listed in section 1. On the

other hand, if $M_{f,WDM} \gtrsim 10^{13} M_{\odot}$ the bulk of galaxy and star formation will likely take place too late relative to the observed star-formation history of the Universe, as discussed below (see also Pierpaoli et al. 1998). Consequently we initially carry out three MR simulations (with $\Omega_b = 0.05$) of the formation of disk galaxy S4 with $k_c = 12.4, 6.2$ and $3.1 h \text{ Mpc}^{-1}$ corresponding to free-streaming masses of $1.9 \times 10^{10}, 1.5 \times 10^{11}$ and $1.2 \times 10^{12} h^{-1} M_{\odot}$ by eqs. (5) and (13). We denote warm dark matter with these characteristics WDM1, WDM2 and WDM3 in the following and the corresponding simulations runs #1-3. Figure 4 shows the specific angular momentum j_{disk} (upper panel) and cooled out gas mass M_{disk} (lower panel) of the central, cold and dense, forming disk (with $R \leq 30 \text{ kpc}$ and $n_H > 0.01 \text{ cm}^{-3}$) as a function of time since Big Bang (at times when central merging is in process, i.e. when a merging satellite is inside of $r = 30 \text{ kpc}$, j_{disk} and M_{disk} are not shown in this and the following figures. Such merging episodes are clearly seen in the figures as steep increases in $M_{disk}(t)$). The observed value of j for Milky Way sized disk galaxies is $j_{obs} \sim 1000\text{-}1500 \text{ kpc km/s}$ - see section 5. As can be seen from Figure 4, the CDM and WDM3 simulations generally have $j \lesssim 200 \text{ kpc km/s}$. Moreover, for the WDM3 simulations cold, dense gas, and hence the basis for star formation, is not formed before $t \sim 4.5 \text{ Gyr}$, corresponding to a redshift $z \sim 1$, in disagreement with the observed star-formation history of the Universe - see, e.g., Madau et al. (1996) and Steidel et al. (1999). The WDM1 and WDM2 simulations look much more promising, both having $j \gtrsim 400 \text{ kpc km/s}$ and for WDM2 even $j > 800 \text{ kpc km/s}$ at present ($z=0$). Moreover, for the WDM1 and WDM2 simulations, gas cools out approximately as early and at the same rate as for the CDM simulation, but as the inflow of gas is more smooth and coherent, considerably larger angular momenta result, as discussed by SLGV99.

Guided by the results above we secondly carry out three MR WDM2 simulations (with $\Omega_b = 0.05$) of the formation of the disk galaxies S1-S3 (runs #4-6). As discussed in SLGV99 one may expect that part of the angular momentum problem is related to numerical effects, in particular angular momentum transport due to artificial viscosity. One would expect this effect to be reduced as the resolution of the simulations is increased. Consequently, we thirdly carry out four WDM2 HR simulations (with $\Omega_b = 0.05$) of galaxies S1-S4 with 8 times the mass resolution (4 times for SPH) of the MR simulations (runs #7-10).

The effects of a background UVX radiation field on disk galaxy formation has been discussed by, e.g., Vedel et al. (1994) and Navarro & Steinmetz (1997). To study the effect of not including a UVX field in the simulations (but still inverse Compton cooling) we fourthly carry out four MR WDM2 simulations (with $\Omega_b = 0.05$) of galaxies S1-S4 without a UVX field (runs #11-14). Finally, to study the effect of having a baryonic fraction of 0.10 rather than 0.05 we carry out four MR WDM2 simulations of galaxies S1-S4 with $\Omega_b = 0.10$ and with a background UVX radiation field (runs #15-18).

Parameters for all the simulations are listed in Table 1.

5. Results

5.1. Disk masses and specific angular momenta

Table 2 presents some global properties of the final collapsed objects in our 18 simulations. The first column is the simulation label, as described in the previous section. Columns 2, 3, and 4 respectively hold the virial mass M_{200} , the virial radius r_{200} , and the circular velocity V_{200} at the virial radius. The numbers N_{gas} and N_{DM} of gas and DM particles inside the virial radius are in columns 5 and 6, and the corresponding masses M_{gas} and M_{DM} in columns 7 and 8. Columns 9, 10, and 11 show the number of gas particles N_{disk} , the corresponding baryonic mass M_{disk} , and the ratio $M_{\text{disk}}/\Omega_b M_{200}$ for the cold disk present at the end of each simulation.

The time evolution of j_{disk} and M_{disk} for the WDM2 MR simulations with $\Omega_b=0.05$ of the forming disk galaxies S1-S4 is shown in Figures 5-8 together with those of the corresponding “passive” CDM simulations (from SLGV99) and of the WDM2 HR simulations of galaxies S1-S4 (though not j_{disk} for galaxy S1 - see below). The WDM2 simulations are clearly producing disks with considerably larger j_{disk} than the CDM simulations, whereas the growth of disk mass M_{disk} is fairly similar for the two types of dark matter. Comparing the WDM2 MR and HR simulations qualitative agreement is found in the j_{disk} and M_{disk} evolution between the two types of simulations. This is gratifying, since the substructure in the forming galaxies with this kind of dark matter in general is resolved even in the MR simulations (with one exception, as discussed below). For any given galaxy, however, $j_{\text{disk}}(t)$ for the HR simulations generally exceeds j_{disk} for the MR simulations. This is particularly evident towards the end of the simulations ($z \sim 0$), where the ratio of the two typically is 1.5-2.5. This strongly suggests that part of the angular momentum problem is due to numerical effects: We have performed TREESPH simulations of (idealized) smooth, disk galaxy forming cooling-flows, in differential rotation in a rigid, spherical halo potential to study the effects of spurious angular momentum transport related to SPH. From these test simulations we find that increased resolution leads to less angular momentum transport and resulting central, cold disks of higher specific angular momentum and that the angular momentum transport is mainly due to the shock capturing, artificial viscosity used in SPH. We also find that going from the standard Monaghan-Gingold viscosity (Monaghan & Gingold 1983) used in this work to the shear-free Balsara (1995) viscosity does not result in higher specific angular momentum disks at a given level of resolution. These issues will be discussed in a future paper - see also the brief discussion in SLGV99.

Galaxy S1 is very different from the others: At about $t \sim 4$ Gyrs the central galaxy develops into a kinematically complex system through accretion of counterrotating hot gas and a cold gas merging event. By then it consists of an inner, high density disk surrounded by an outer, more extended but lower density counterrotating disk. In the MR simulations the spin vector of the inner disk flips around and aligns itself with that of the outer disk during the next 2-4 Gyrs. In contrast, the inner disk in the HR simulation does not “flip” relative to the outer during the remaining ~ 9 Gyrs of the simulation. This clearly indicates that the gasdynamical (and perhaps also gravitational) resolution is not sufficient to resolve the long-lived, discontinuous kinematics. We chose to plot and give values for the specific angular momenta of the final disks formed in the MR simulations of galaxy S1, as these disks are kinematically relaxed. But given the possible resolution problems in these simulations, we do not use the results in any of the following quantitative estimates of the angular momentum properties of disks formed in WDM simulations. We do not give specific angular momenta results for the HR simulation of galaxy S1, as this system is kinematically unrelaxed during most of the simulation, including the final state. Given the observational variety of galaxies, including some with counterrotating disks (e.g., Thakar & Ryden 1998 and references therein), we find it almost reassuring that not *all* simulated galaxies end up as extended, kinematically coherent disks, as long as most do!

The time evolution of j_{disk} and M_{disk} of galaxies S1-S4 for the WDM2 MR simulations with $\Omega_b=0.05$ and no UVX background radiation field is shown in Figure 9 (runs #11-14). Not surprisingly, the final disk masses are somewhat larger (on average by about 25%) than for the corresponding runs with a UVX field. This is due to the somewhat more efficient radiative cooling and lack of photo-heating in the absence of a UVX field. Moreover, the specific angular momenta of the final disks are on average about 45% larger than for the runs with a UVX field - we comment on this below.

Finally, the time evolution of j_{disk} and M_{disk} of galaxies S1-S4 for the WDM2 MR simulations with $\Omega_b=0.10$ and a UVX field is shown in Figure 10 (runs #15-18). The final disk masses are about a factor of 2.5 times those of the corresponding $\Omega_b=0.05$ runs. This is not far from the factor of about $2^{3/2}$ expected from cooling flow theory assuming an isothermal dark matter potential (Sommer-Larsen 1991). The specific angular momenta of the final disks are about a factor 2.8 times those of the corresponding $\Omega_b=0.05$ runs. This is significantly more than the factor of about $2^{1/2}$ expected from cooling flow theory (Sommer-Larsen 1991) - we also comment on this below.

In order to compare the masses and specific angular momenta of the final disks to observations a characteristic circular velocity, V_c , is assigned to the model disk galaxies in the following way: Courteau (1997) compared for Tully-Fisher applications optical rotation

curves with 21 cm linewidths of disk galaxies. He found from the data that the circular velocity, $V_{2.2}$, at 2.2 exponential disk scale-lengths from the center (where the circular velocity of the disk alone peaks) gives the best match to the 21 cm linewidths. Since the disks of our model galaxies are not perfectly exponential and generally still somewhat too concentrated compared to observations we determine $V_c = V_{2.2}$ iteratively. Given the dark matter part of the rotation curve and the disk mass, both taken from the simulations, and using the observational relation between the median exponential disk scale-length and the characteristic circular velocity

$$\bar{R}_d = 1.9 \text{ } h^{-1} \left(\frac{V_c}{200 \text{ km/s}} \right)^{1.05} \text{ kpc} \quad (14)$$

(SLGV99), $V_c = V_{2.2}$ is determined in the following way: Starting from an initially adopted $V_{2.2}$ ($= V_c$) the corresponding characteristic scale-length is determined using (14). Assuming that the “real” disk is exponential and given the disk mass M_{disk} and scale-length R_d the disk part of the rotation curve is determined. This is then added in quadrature to the dark matter part of the rotation curve and finally $V_{2.2}$ is determined from the combined rotation curve. This value is then used as input to the above procedure, which is repeated until the input $V_{2.2}$ equals the output $V_{2.2}$.

As the baryonic mass is somewhat more centrally concentrated than the exponential disk of the same mass the dark matter halo may be somewhat too “pinched”. This means that $V_c = V_{2.2}$ determined in this way actually is an upper limit in this connection. We estimate, however, that the effect of the extra pinching is quite small: As an example we show in Figure 11 the dark matter part of the rotation curve $V_{c,DM}(R)$ (upper panel) and $M_{disk}(R)$ (lower panel) for the four simulations runs #4, 7, 11 and 15 of galaxy S1 at $z=0$. As can be seen from the Figure, the final dark matter halo rotation curves are fairly insensitive to the quite different amounts of baryonic mass inside of $R_{2.2} \simeq 10-15$ kpc for $h=0.5$. Another possible concern is that part of the cooled-out mass may end up in a central component/bulge, which may change the estimate of $V_{2.2}$. Assuming that no more than 20% of the baryonic mass is in such a component for Sb-Sd galaxies (see section 5.2) we find, however, that this leads to an average increase of $V_{2.2}$ of no more than about 1%, so we neglect this effect as well. Finally, for the arguments given in this paper, we can neglect the effects of a possible truncation of the disk at $\sim 4 R_D$ (van der Kruit & Searle 1982).

The specific angular momenta j_{disk} and iteratively determined characteristic circular velocities $V_c = V_{2.2}$ of the final disks in the 18 simulations are given in Table 3. The Table also lists our computed values for the dimensionless spin parameter $\lambda \equiv J|E|^{1/2}/GM^{5/2}$ (column 3) evaluated at the *infall radius* r_{inf} (column 5). This radius is defined by $M_{DM}(r_{inf})/(1 - \Omega_b) = M_{disk}/\Omega_b$, and is of order 120-200 kpc in all our runs. It represents a

characteristic radius, at the present time, of the dark matter originally associated with the amount of gas currently in the disk. In Figure 12 we show the “normalized” specific angular momenta $\tilde{j}_{disk} = j_{disk}/V_c^2$ of the final disk galaxies formed in all WDM2 runs (except run #7) as a function of V_c . As argued by SLGV99 one expects \tilde{j}_{disk} to be almost independent of V_c on both theoretical and observational grounds. Also shown in the figure is the median “observed” value of \tilde{j}_{disk} , calculated using equation (14) and

$$\tilde{j} = \frac{j}{V_c^2} = \frac{1.68R_d}{V_c} \quad (15)$$

(SLGV99), and the observational 1- σ and 2- σ contours.

For the MR WDM2 simulations of galaxies S2-S4 with $\Omega_b = 0.05$ and including effects of a UVX field the median $j \simeq 500$ kpc km/s and the median \tilde{j}_{disk} is 0.61 ± 0.11 dex below the “observed” value, corresponding to a factor of 4. This is almost an order of magnitude better than what is obtained with “passive” CDM simulations - see, e.g., Navarro & Steinmetz (1997) and SLGV99.

For the HR WDM2 simulations of galaxies S2-S4 with $\Omega_b = 0.05$ and including effects of a UVX field the median $j \simeq 940$ kpc km/s and the median \tilde{j}_{disk} is (just) 0.32 ± 0.07 dex below the observed, corresponding to a factor of two. As noted above this strongly suggests that part of the angular momentum problem is related to numerical problems.

For the MR WDM2 simulations of galaxies S2-S4 with $\Omega_b = 0.05$ and no UVX field the median $j \simeq 730$ kpc km/s and the median \tilde{j}_{disk} is 0.45 ± 0.13 dex below the observed, corresponding to a factor of 2.8. We interpret the larger specific angular momenta obtained for the final disks relative to the simulations including a UVX field as being due to the combination of two effects: a) The more efficient cooling results in more high angular momentum gas from the outer regions of the halo to be deposited onto the disk during the simulations - as discussed by Navarro & Steinmetz (1997) and b) This increased cooling efficiency and lack of photo-heating does *not* lead to the cool-out of a very large number of gas clouds in small mass dark matter halos ($V_c \lesssim 40$ km/s, Efstathiou 1992, Quinn et al. 1996) in our WDM2 simulations compared to CDM, because the number of such small dark matter halos is greatly reduced for WDM2 relative to CDM. This could otherwise lead to an increased angular momentum transfer from the gas clouds to the main dark matter halo by dynamical friction, as discussed in section 1.

The first of the two effects discussed above is even more pronounced in the MR WDM2 simulations with $\Omega_b=0.10$ and a UVX field due to the ~ 4 times higher cooling rates compared to the similar simulations with $\Omega_b=0.05$: For galaxies S2-S4 the median $j \simeq 1380$ kpc km/s and the median \tilde{j}_{disk} is (just) 0.36 ± 0.12 dex below the observed corresponding to a factor of 2.3.

Summarizing, we find that increasing the mass resolution by a factor of 4 (8 for DM) leads to the formation of disk galaxies with final specific angular momenta, which are almost a factor two larger than those of the otherwise identical medium resolution simulations and just a factor of about two smaller than those of observed disk galaxies. Moreover, the median value of the spin parameter λ for the three HR simulation galaxies S2-S4 is 0.039. Assuming a theoretical median value of λ of 0.05 (Barnes & Efstathiou 1987; Heavens & Peacock 1988) the discrepancy is further reduced to a factor of 1.6. Given that the rather modest increase in mass resolution reduces the discrepancy by almost a factor of two, we find it plausible that the remaining factor of ~ 1.6 may be gained by increasing the mass resolution even further, but this obviously has to be checked with very high resolution simulation. Furthermore we also find that going from a baryonic fraction of $f_b=0.05$ to $f_b=0.10$ (which may well be more realistic) also improves the situation considerably for the MR simulations, as discussed above. To illustrate this we show in Figure 13 a face-on view and in Figure 14 an edge-on view of the final galaxy formed in run # 18 (this has the largest specific angular momentum of all the galaxies formed, $j_{disk} \simeq 2000$ kpc km/s). Further, in Figure 15 we show the (azimuthally averaged) surface density profiles of the final disks in runs #15-18. Clearly, it is no longer a problem to form extended disks in cosmological simulations!

All in all we find that the disk galaxy angular momentum problem can be significantly alleviated (and we speculate: perhaps even completely resolved) by going to the WDM cosmological structure formation scenario, provided that the WDM free-streaming mass is $M_{f,WDM} \sim 10^{11}h^{-1}M_\odot$ within about a factor of three if $\Omega_M=1$. We shall touch briefly on the $\Omega_M < 1$ case in section 7.

5.2. The Tully-Fisher relation and mass-to-light ratios of disk galaxies

In Figure 16 we show $M_{disk}(V_c)$ of the final disk galaxies formed in all 16 WDM2 runs together with the I -band Tully-Fisher relation (TF) of Giovanelli et al. (1997) for $h=0.5$, converted to mass assuming mass-to-light ratios $(M/L_I) = 0.25, 0.5$ and 1.0 in solar units (used throughout). The slope of the “theoretical” TF matches that of the observed very well for a constant mass-to-light ratio, and for $h=0.5$ the required $(M/L_I) \simeq 0.6$. This value is in fair agreement with some estimates of the (M/L_I) of disk galaxies in the literature and somewhat low relative to others: Persic & Salucci (1992) find a dynamical estimate of $(M/L_B) = 1.24h$ for disks, corresponding to $(M/L_B) = 0.62$ for $h=0.5$ or $(M/L_I) \simeq 0.4$ assuming Sbc type colours (see also Persic et al. 1996). Syer et al. (1997) find $(M/L_I) < 1.9h$ from disk stability arguments corresponding to $(M/L_I) < 0.95$ for

$h=0.5$. The (M/L) s obtained from stellar population synthesis depend strongly on the assumed initial mass function (IMF), in particular the effective lower mass cut. Recent determinations of the (M/L) of disk galaxies based on what is thought to be realistic IMFs range from $(M/L_B) \simeq 1.9$ (Fukugita et al. 1998), corresponding to $(M/L_I) \simeq 1.3$, to $(M/L_I) \simeq 1.0$ for Milky Way sized disk galaxies and slightly less for smaller galaxies (Boissier & Prantzos 1999). Adopting (more realistically) $h=0.7$ increases the dynamical estimates to $(M/L_I) \simeq 0.6$ (Persic & Salucci) and $(M/L_I) < 1.3$ (Syer et al.), bringing them in better agreement with the stellar population synthesis ones. One can show that the final virial mass and final cooled-out disk mass will scale approximately as h^{-1} for the simulations, everything else being unchanged. As the inferred absolute luminosity of the disk galaxies scales as h^{-2} , one would expect (M/L_I) to increase by about 40% by going from $h=0.5$ to $h=0.7$. However, since the characteristic length-scale of the CDM (and hence WDM) power-spectrum scales as h^{-2} (for fixed Ω_M) and not h^{-1} the magnitude of linear density fluctuations on galactic mass scales is approximately 30% larger for $h=0.7$ than for $h=0.5$, given the same value of σ_8 . To test the effect of this we carry out four MR WDM2 simulations (with $\Omega_b=0.05$ and including the UVX field) of the formation of disk galaxies S1-S4 with $h=0.7$, but otherwise similar to runs #2 and #4-6 (in particular with $\sigma_8=0.5$, as before). For the resulting 4 galaxies we find $(M/L_I) = 0.62 \pm 0.02$ compared to $(M/L_I) = 0.54 \pm 0.02$ for the similar $h=0.5$ runs, an increase of (only) $11 \pm 5\%$. Assuming this modest increase to be generally applicable, we would expect a $(M/L_I) \simeq 0.7$ for WDM2 simulations with $h=0.7$ ($\Omega_M = 1, \Omega_\Lambda = 0, \sigma_8 = 0.5$).

All in all, the result of our WDM2 simulations suggest that values of $(M/L_I) \simeq 0.6-0.7$ for $h=0.5-0.7$ are required to match the observed Tully-Fisher relation. Such values of (M/L_I) for disks are fairly consistent with dynamical estimates, but somewhat low compared to stellar population synthesis values.

Steinmetz & Navarro (1999) and Navarro & Steinmetz (2000) carried out GRAPESPH, SCDM and Λ CDM simulations of disk galaxy formation. They found that a $(M/L_I) \simeq 0.5$ is required to match the results of the simulations to the observed I -band Tully-Fisher relation. Their required (M/L_I) value is comparable to, though somewhat lower than ours. Since this difference could be related to the use of different types of dark matter, we determined the (M/L_I) required to match the results of our CDM simulations corresponding to runs #2 and #4-6 (described in SLGV99) to the observed TF relation. We find a $(M/L_I) = 0.51 \pm 0.04$ for our CDM simulations compared to $(M/L_I) = 0.54 \pm 0.02$ for the corresponding WDM2 simulations ($h=0.5$), so there is no indication that going from CDM to WDM leads to larger (M/L_I) s. It is not clear what leads to the (small) difference between the results of the above authors and ours, but it may be related to the use of different normalizations, σ_8 , of the power spectra.

We now estimate a general upper limit to the (M/L_I) of disk galaxies by assuming that disks are “maximal”, i.e. as dominant in the inner part of the galaxies as possible given the rotation curve constraints: Maximal disk galaxies have $\gamma \equiv V_{2.2,D}/V_{2.2} \simeq 0.85$ (e.g., Sackett 1997), where $V_{2.2,D}$ is the (peak) rotation velocity of the disk alone at $R_{2.2}$. The disk mass can be expressed as $M_D = f_D M_b$, where M_b is the total, baryonic disk galaxy mass (central component + bulge + disk - neglecting the stellar halo and, for notation, assuming that dark matter is non-baryonic). For an exponential disk

$$V_{2.2,D} = 0.62 \sqrt{\frac{GM_D}{R_D}} . \quad (16)$$

Using this, equation (14) and the definition of γ we then obtain

$$M_b = 4.2 \cdot 10^{10} h^{-1} \left(\frac{f_D}{0.8} \right)^{-1} \left(\frac{\gamma}{0.85} \right)^2 \left(\frac{V_c}{200 \text{ km/s}} \right)^{3.05} M_\odot . \quad (17)$$

Following Giovanelli et al. (1997) the I -band TF relation can be expressed as

$$L_I = 2.1 \cdot 10^{10} h^{-2} \left(\frac{V_c}{200 \text{ km/s}} \right)^{3.07} L_{I,\odot} , \quad (18)$$

so the I -band mass-to-light ratio of a disk galaxy is given by

$$(M/L_I) = 2.0 h \left(\frac{f_D}{0.8} \right)^{-1} \left(\frac{\gamma}{0.85} \right)^2 \left(\frac{V_c}{200 \text{ km/s}} \right)^{-0.02} M_\odot . \quad (19)$$

Adopting $f_D \gtrsim 0.8$ for Sb-Sd galaxies (e.g., Broeils & Courteau 1997), $\gamma \lesssim 0.85$ (maximal or sub-maximal disks) and neglecting the very weak V_c dependence, we obtain

$$(M/L_I) \lesssim 2.0h \quad (20)$$

for intermediate to late type disk galaxies, which for $h=0.7$ translates into $(M/L_I) \lesssim 1.4$. This is likely to be a generous upper limit as disk galaxies may well be sub-maximal ($\gamma < 0.85$) - see, e.g., Courteau & Rix (1999). The estimated upper limit in equation (20) is consistent with the various dynamical and spectrophotometric estimates discussed above, for $h \sim 0.7$.

5.3. The total baryonic mass of the Milky Way as a constraint on disk galaxy formation simulations

Another observational check of the results is obtained by comparing the final disk masses as a function of V_c with the observed, baryonic mass of the Milky Way: Flynn &

Fuchs (1994) find a dynamically determined local disk surface density of $52 \pm 13 M_{\odot} / \text{pc}^2$, out of which about 20-25% is gas. Assuming that the Galactic disk is exponential and that the Sun is situated at $R=8$ kpc, the total disk mass can be calculated as a function of the exponential scale-length R_D . The result is shown in Figure 18 (solid line) together with the observational $1-\sigma$ contours. This provides a lower limit to the baryonic mass of the Milky Way (the radial gas surface density profile is somewhat shallower than that of the stars, but the effect of this on the total disk mass is small, especially since only about 10% of the baryonic mass of the Milky Way is gas).

An upper limit can be obtained by taking into account the mass of the central component (CC)/bulge also. This mass component is highly centrally concentrated, so for our purpose we simply assume that it is located at the center and characterized by a Keplerian rotation curve. We now demand that the combined disk/CC/bulge rotation curve should not exceed the observed value of $\lesssim 200$ km/s at $R=3$ kpc (Rholfs et al. 1986) and in this way obtain the CC/bulge mass upper limit shown in Figure 18 (short-dashed line) together with lower and upper $1-\sigma$ contours (long-dashed lines) corresponding to the upper and lower ones for the disk mass. The combined disk/CC/bulge upper $1-\sigma$ mass limit for the Milky Way is shown as a heavy solid line in the Figure. We conclude that the baryonic mass of the Milky Way is somewhere in the range $3 - 7 \times 10^{10} M_{\odot}$ with a likely value of about $5 \times 10^{10} M_{\odot}$. We adopt a characteristic circular velocity of the Galaxy of $V_c = 220$ km/s with a 10% uncertainty and plot the result in Figure 16. Clearly, our results are compatible with the Milky Way baryonic mass constraint for $h=0.5$ (as well as $h=0.7$ - see below), given the uncertainties.

Our determination of the baryonic mass of the Milky Way provides an effectively independent way of estimating the I -band mass-to-light ratio of a disk galaxy: Assuming $M_{b,MW} = 5 \pm 2 \times 10^{10} M_{\odot}$, $V_{c,MW} = 220 \pm 20$ km/s, $h = 0.7 \pm 0.1$ and that the I -band luminosity of the Milky Way is given by equation (18) with a 40% uncertainty (approximately the dispersion in luminosity at a given V_c of the TF relation), and adding all uncertainties in quadrature yields $(M/L_I)_{MW} = 0.87 \pm 0.57$. This further strengthens the case for a low value of the typical (M/L_I) of disk galaxies ($(M/L_I) \lesssim 1$).

6. Physical candidates for warm dark matter.

Warm dark matter is usually considered as exotic in comparison with “normal” cold dark matter. However warm dark matter particles (we will call them *warmons* in what follows) are by no means less natural than cold dark matter ones. Of course naturalness is a rather vaguely defined notion and we assume that some particles are natural candidates for

dark matter if their existence is predicted or requested by the theory independently from dark matter problem. The most popular candidates for cold dark matter are either lightest supersymmetric particles with the mass of a few hundred GeV which would be stable if the so called R-parity is conserved, or very light axions with the mass about 10^{-5} eV. There are several equally natural candidates for warm dark matter particles as well. Their properties are fixed by the condition that they should be stable on the cosmological time scale (the life-time should be larger than the universe age, $\tau_w > t_U \approx 10^{10}$ Gyr) and their mass should be sufficiently light $m_w \sim 1$ keV, to give a free-streaming mass of $\sim 10^{11} M_\odot$, cf. equation (6) (in this section we use the system of units with $c = \hbar = k_B = 1$). The simplest possibilities for the warmons are either massive neutrinos or pseudo-Goldstone bosons.

It is natural to start with massive neutrinos, firstly, because neutrinos, in contrast to other possible dark matter particles are known to exist and, secondly, they may be massive. However the interpretation of atmospheric neutrino anomaly by oscillations between ν_μ and ν_τ or a sterile neutrino ν_s demands a very small mass difference of oscillating neutrinos, $\delta m^2 \approx 0.01$ eV² (Super-Kamiokande Collaboration 1998). An explanation of the solar neutrino deficit by neutrino oscillations also demands a very small mass difference, now between ν_e and some other active or sterile neutrinos (see, e.g., Bahcall et al. 1998). Other neutrinos may have masses in the keV range and be warmons: An example of warm dark matter created by sterile neutrinos was recently considered in Dolgov & Hansen 2000.

According to the Gerstein-Zeldovich (1966) and Cowsik & MacLelland (1972) neutrinos with the *normal weak interactions* have the cosmological mass density, $\Omega_\nu h^2 = m_\nu / 94\text{eV}$ so keV neutrinos would over-close the universe. A possible way to save neutrinos as warmons is to assume that they have a new stronger interaction, diminishing their number density by one-two orders of magnitude Correspondingly the cross-section of their annihilation should be

$$\sigma_{ann} \approx \frac{10}{94\text{eV} m_{Pl} \Omega_w h^2} \approx 4 \cdot 10^{-39} \text{cm}^2 / (\Omega_w h^2) \quad . \quad (21)$$

Due to this interaction the neutrinos would decouple at $T \approx m_\nu / 5$. Until then their mean-free path is determined by the annihilation and would be considerably shorter than the horizon. This could reduce the scale at which perturbations are erased in comparison with more conventional dark matter, which is free-streaming for $T \gtrsim m_\nu$. However in this model there exists a new mechanism for dissipation of perturbations at small scales, namely $\nu\nu$ -annihilation. The larger the number density of neutrinos the stronger the annihilation and thus neutrinos disappear faster in regions with higher neutrino density, reducing the density contrast.

Elastic scattering of neutrinos (or other warmons, e.g. light scalars) may be stronger

than the annihilation and the particle mean free path may be much smaller than galactic scales. This could lead to a lowering of the central concentration of dark matter halos - see, e.g., Spergel & Steinhardt (1999).

Another warmon model can be realized with early decoupled keV particles whose number density is diluted by a subsequent entropy release. Hence the present day ratio of the number densities of warmons and CMB photons would be:

$$(n_w/n_\gamma)_0 = 43g_w/11g_{dec} , \quad (22)$$

where g_{dec} is the effective number of particle degrees of freedom at warmon decoupling and $g_w = (n_w/n_\gamma)_{dec} \approx 1$. The contribution of such warmons to the present day “mass density” $\Omega_w h^2$ would be

$$\Omega_w h^2 = 1.5 \cdot 10^2 m_w (g_w/g_{dec}) \quad (23)$$

where the warmon mass is expressed in keV. This expression is very similar to equation (4) in section 2 for $g_w \sim 1$. In the minimal standard model the number of particle species above the electroweak scale is $g_{dec} = 107.75$ so the suppression factor is too small to get a small $\Omega_w h^2 \sim 0.1$ with keV mass warmons. Only for very weak interactions and if the rank of the unification group is sufficiently high the entropy suppression factor would be large enough to permit keV warmons with $\Omega_w h^2 \sim 0.1$. Another mechanism of a large entropy release could be cosmological first order phase transitions.

In the case of earlier decoupled particles their momentum distribution would be considerably softer so they would have a smaller free-streaming scale. The ratio of the warmon temperature, when they are relativistic, to the photon temperature can be expressed as:

$$\frac{T_w}{T_\gamma} = \left(\frac{43}{11g_d} \right)^{1/3} = 0.3 \left(\frac{\Omega_w h^2}{g_w m_w} \right)^{1/3} . \quad (24)$$

The physical warmon path in the expanding reference frame is:

$$l_w = 2.6 \cdot 10^6 \text{ sec } m_w^{-8/3} (\Omega_w h^2 / g_w)^{2/3} . \quad (25)$$

The corresponding comoving free-streaming scale $R_{f,w}$ is given by $(1 + z_w)l_w$, where

$$(1 + z_w) = \frac{T_\gamma}{T_\gamma^{(0)}} = \frac{m_w^{4/3}}{0.9T_\gamma^{(0)}} \left(\frac{g_w}{\Omega_w h^2} \right)^{1/3} = 4.7 \cdot 10^6 m_w^{4/3} \left(\frac{g_w}{\Omega_w h^2} \right)^{1/3} , \quad (26)$$

and $T_\gamma^{(0)} = 2.4 \cdot 10^{-7}$ keV (corresponding to 2.73 K) is the present temperature of the CMB. Hence:

$$R_{f,w} = (1 + z_w)l_w = 0.23 (g_{dec}/100)^{-4/3} (\Omega_w h^2)^{-1} g_w \text{ Mpc} , \quad (27)$$

very similar to equation (3) in section 2 for $g_w \sim 1$.

A generic theoretical problem is the required smallness of the warmon mass. We know that, though do not understand why, most “normal” neutrinos probably are *too* light, so to be warmons, they must either possess stronger than normal weak interactions or vice versa, be almost sterile. A possible example of the latter are the right-handed neutrinos considered by Malaney et al. (1995) and Colombi et al. (1996).

If neutrinos are not WDM particles, then the next best candidate is probably the majoron (Berezinsky & Valle 1993, Babu et al. 1993, Dolgov et al. 1995). Majorons could quite naturally have a mass in the keV range and could give $\Omega_w h^2 \sim 0.1$. If majorons indeed exist, they could either be warmons or would open such a possibility to neutrinos because their coupling to $\bar{\nu}\nu$ introduces a new interaction that would permit to avoid the Gerstein-Zeldovich limit.

There is another possible way of cosmological creation of pseudo-Goldstone bosons, through a phase transition. In this case the particles are produced at rest and a mechanism to warm them up is required. This could be realized if they have a sufficiently strong self-interaction, λJ^4 (where λ is the coupling constant and J is the majoron field). Majorons would predominantly disappear in $4J \rightarrow 2J$ -reactions. Thus this process not only reduces the number density of majorons but also heats them up. The freezing of species by $4 \rightarrow 2$ or $3 \rightarrow 2$ -reactions and properties of the corresponding dark matter has been considered by Dolgov (1980), Carlson et al. (1992), Machacek et al. (1994), de Laix (1995) and Dolgov et al. (1995). Depending upon the efficiency of the cooling and on the initial majoron momentum distribution this model would supply dark matter somewhat warmer or colder than warm.

It is possible that both thermal and phase transition mechanisms are effective, so that the same particles form both cold and warm dark matter. Thus, compared to CDM, one could have a smaller, but *non-vanishing* power on mass scales less than the WDM free-streaming scale ($\sim 10^{10}\text{-}10^{11} M_\odot$). Another case of interest is that some neutrino species are heavier than majorons and decay into majorons and lighter neutrinos. This was considered in several papers dealing with unstable dark matter - see, e.g., Dolgov (1999) and references therein. One may also keep neutrinos rather heavy (in the MeV range), unstable and relatively short-lived, while keV majorons, produced by neutrino decays when the number density of neutrinos was already Boltzmann suppressed, would be dark matter particles. According to e.g. Dolgov et al. 1997 a conflict with big bang nucleosynthesis can be avoided. A new zoo of interesting candidates for dark matter particles is opened up if mirror or shadow worlds exist. A list of references and a discussion of the subject can be found, e.g., in Dolgov (1999). Shadow world neutrinos, as considered by Berezhiani &

Mohapatra (1995) and Berezhiani et al. (1996) would look in our world as sterile ones and might have a keV mass. Finally, new dark matter particles, that might be warmons, have been recently considered by Garriga & Tanaka (1999), Arkani-Hamed et al. (1999) and Csaki et al. (1999) in the framework of multidimensional cosmologies. Phenomenologically they are rather similar to shadow particles.

In summary, there are plenty of particle physics candidates for warmons. Their properties and initial momentum distributions may be significantly different. They could be self-interacting or sterile, long-lived or absolutely stable. To mention a few, they could be neutrinos with weaker or stronger couplings than normal, majorons (light pseudo-Goldstone bosons) or shadow or mirror world neutrinos.

7. Discussion and conclusions

In conclusion we find that the disk galaxy angular momentum problem can be considerably alleviated (and we speculate: perhaps even completely resolved) by going from the CDM to the WDM cosmological structure formation scenario without having to resort to star-burst driven feedback processes at all. The main reason for this is that the inflow of gas onto the forming disk is more smooth and coherent for WDM than for CDM, resulting in considerably larger disk angular momenta, as discussed by SLGV99.

For $\Omega_M=1$ our results suggest that this requires the WDM free-streaming mass to be $M_{f,WDM} \sim 10^{11} h^{-1} M_\odot$ within about a factor of three, indicating that extreme fine-tuning is not required. This range of characteristic free-streaming masses corresponds to characteristic wavenumbers $k_c \sim 5-10 h \text{ Mpc}^{-1}$. For wavenumbers about 2-3 times larger than this the WDM power spectrum is significantly reduced relative to the CDM one, cf. Figure 1. In the interesting work by Croft et al. (1999) the linear power spectrum is determined “observationally” from the Ly α forest in spectra of quasars at $\langle z \rangle = 2.5$ for wavenumbers in the range $0.3-0.5 \lesssim k \lesssim 2-3 h \text{ Mpc}^{-1}$. In this range of wavenumbers the measured $P(k)$ is found to compare well with CDM power spectra. If this method can be pushed to about 4 times larger wavenumbers, it would be possible to test directly the hypothesis that dark matter is warm, with the characteristics proposed in this work, rather than cold. In fact, McDonald et al. (1999) have been able to push the method to about twice as large wavenumbers by using high dispersion spectra of quasars at somewhat larger redshifts (see also Nusser & Haehnelt 1999), but this is probably as far as one can get using the Ly α forest method (R. Croft, private communication). Another, but much more indirect way of obtaining information about power on small scales may come from the comparison of observations and models of damped Ly α systems - see, e.g., Haehnelt

et al. (1998) and McDonald & Miralda-Escudé (1999).

Currently there are many indications that Ω_M probably is less than unity, $\Omega_M \simeq 0.3$, say. For such OWDM as well as Λ WDM models the cluster normalized value of σ_8 will be $\simeq 1$, rather than 0.5 for the $\Omega_M=1$ considered in this paper. Also, the late linear growth is slower in the low Ω models. Taking this together implies that the density fluctuations are about 1.5-2 times larger at redshifts $z \gtrsim \Omega_M^{-1} - 1$ and consequently that galaxy formation is somewhat faster and more intense in low Ω_M models. For such cosmologies it therefore seems reasonable to assume that the WDM free-streaming mass-scales, which will allow large, high specific angular momentum disks to form, will be comparable to, but no less than the ones found in this work for $\Omega_M=1$. From this constraint and equation (6) it follows that the mass of the warm dark matter particle(s) has to be of the order 1 keV with a fairly weak dependence on Ω_{WDM} .

We find a slope of our “theoretical” Tully-Fisher relation which matches that of the observed I -band TF relation very well. In terms of the normalization of the TF relation we find agreement provided that the mass-to-light ratio of disk galaxies is $(M/L_I) \simeq 0.6 - 0.7$ for $h=0.5-0.7$. We argue that this is in reasonable agreement with various recent estimates of (M/L_I) , including two given in section 5.2 of this paper. The discrepancy of a factor of $\sim 4 - 5$ in absolute luminosity found by Steinmetz & Navarro (1999) and Navarro & Steinmetz (2000) in matching the observed TF relation, using similar kinds of CDM disk galaxy formation simulations, is at least partly caused by the adoption of a larger mass-to-light ratio ($(M/L_I) \sim 2$) by these authors. We find no indication that going from CDM to WDM increases the I -band mass-to-light ratio required for the model disk galaxies to match the observed TF relation. This is agreement with the findings of Moore et al. (1999b) that a suppression of power on small scales similar to the one discussed in this paper does not change the structure of the resulting dark matter halos. However, in their simulations as well as ours the possibility of having WDM particles, which initially have a non-zero velocity dispersion (due to free-streaming) was not taken into account.

A potential problem for the WDM scenario might be a lack of a sufficient rate of early galaxy formation to match observations: Lyman break galaxies are routinely found at redshifts 3-4 and galaxies have been detected at even higher redshifts, with a possible current record of $z=6.7$ (Chen, Lanzetta & Pascarelle 1999). Assuming that galaxies form from n - σ peaks, where $n \sim 2-3$ (e.g., Ryden & Gunn 1987), and using linear theory it follows that the typical formation redshift of galaxies of mass M will be $z_f \simeq n\sigma(M; z=0)/\delta_c - 1$, where $\delta_c=1.69$ (see White 1993). From Figure 2 it follows that for the characteristic WDM free-streaming masses relevant for this work, smaller galaxies ($M \lesssim 10^9-10^{10} M_\odot$) will form from 2- σ peaks at typical redshifts $z_f \sim 4-5$ and from (rarer) 3- σ peaks at $z_f \sim 6-8$ and

larger galaxies somewhat later (but not later than in CDM models as $\sigma(M)$ is almost the same in the WDM1, WDM2 and CDM models for $M \gtrsim 10^{11} M_{\odot}$). For low Ω_M cosmologies the formation redshifts would be expected to be even higher than this, so qualitatively the WDM scenario does not seem to be in trouble on this point. Moreover, Schaeffer & Silk (1988) found that warm dark matter can provide a galaxy distribution that is close to observed galaxy counts, provided $\Gamma \equiv \Omega_M h > 0.1$, which is likely to be the case. In particular they found that in the warm dark matter structure formation scenario small-scale objects ($M \lesssim 10^{10} M_{\odot}$) are not overproduced, contrary to what may be the case for CDM, cf. section 1.

A general problem for $\Omega_M=1$ models is major (mass ratios $\sim 1:4$ or more), late merging events, which potentially can be fatal for the fragile, stellar disks. Such late merging events also occur in our WDM simulations of galaxies S2-S4 at redshifts $z=0.2-0.4$. This provides yet another reason for going to low Ω_M models, since such merging would be expected to take place faster and earlier, leaving more time afterwards for the disks to grow smoothly and steadily from cooling flows and to form stars out of the cool gas.

Finally, from a particle physics point of view, there are plenty of candidates for warmons. Their properties and initial momentum distributions may be significantly different. They could be self-interacting or sterile, long-lived or absolutely stable. It is even possible that the *same* particles form both cold and warm dark matter. If so, the exciting possibility exists, that compared to CDM one could have smaller, but non-zero power on mass scales less than the WDM free-streaming scale ($\sim 10^{10}-10^{11} M_{\odot}$).

To mention a few WDM particle candidates in summary, they could be neutrinos with weaker or stronger couplings than normal, majorons (light pseudogoldstone bosons) or shadow or mirror world neutrinos.

In closing, given the success of WDM scenario in solving the angular momentum problem and possibly other problems related to galaxy formation and structure, N-body and more hydro/gravity simulations should be undertaken in various cosmologies to bring the WDM scenario on a more rigorous footing.

We have benefited from the comments of Per Rex Christensen, Rupert Croft, Julien Devriendt, Chris Flynn, Fabio Governato, Martin Götz, Ben Moore, Bernard Pagel, Massimo Persic, Elena Pierpaoli, Joel Primack, Örnólfur Rögnvaldsson, Jens Schmalzing, Joe Silk, Henrik Vedel and the referees. This work was supported by Danmarks Grundforskningsfond through its support for the establishment of the Theoretical Astrophysics Center. AD

thanks the Issac Newton Institutue for Mathematical Science for its hospitality during the completion of this work.

REFERENCES

Arkani-Hamed, N., Dimopoulos, S., Dvali, G., & Kaloper, N. 1999, hep-th/9911386

Babu, K. S., Rothstein. I. Z., & and Seckel, D. 1993, Nucl. Phys. B403, 725

Bahcall, J. N., Krastev, P. I., & Smirnov, A. Yu. 1998, Phys.Rev. D58, 096016

Bardeen, J., et al. 1986, ApJ, 304, 15

Barnes, J., & Efstathiou, G. 1987, ApJ, 319, 575

Berezhiani, Z. G. & Mohapatra, R. N. 1995, Phys. Rev. D52, 6607

Berezhiani, Z. G., Dolgov, A. D., & Mohapatra, R. N. 1996, Phys. Lett. B375, 26

Berezinsky, V., & Valle, J. W. F. 1993, Phys. Lett. B318, 360

Blumenthal, G., Pagels, H., & Primack, J. R. 1982, Nature, 299, 37

Boissier, S., & Prantzos, N. 1999, MNRAS, in press (astro-ph/9909120)

van den Bosch, F. C., et al. 1999, AJ, submitted (astro-ph/9911372)

Broeils, A. H., & Courteau, S. 1997, in Dark and Visible Matter in Galaxies and Cosmological Implications, ed. M. Persic and P. Salucci (ASP, San Francisco), p. 74

Burkert, A. 1995, ApJ, 488, L55

de Blok, W. J. G., & McGaugh, S. S. 1997, MNRAS, 290, 533

Carlson, E. D., Machacek, M. E., & Hall, L. J. 1992, ApJ, 398, 43

Caso, C., et al. 1998, European Phys. J., C3, 1

Chen, H. W., Lanzetta, K. M., & Pascarelle, S. 1999, Nature, 398, 586

Choi, K., & Santamaria, A. 1990, Phys. Rev. D42, 293

Colombi, S., Dodelson, S., & Widrow, L. M. 1996, Ap. J. 458, 1

Courteau, S. 1997, AJ, 114, 2402

Courteau, S., & Rix, H. W. 1999, ApJ, 513, 561

Cowsik, R., & MacLelland, J. 1972, Phys. Rev. Lett. 29, 669

Croft, R. A. C., et al. 1999, ApJ, 520, 1

Csáki, C., Graesser, M., Randall, L., & Terning, J. 1999, hep-th/9911406

Dalcanton, J. J., & Hogan, C. J. 2000, astro-ph/0004381

Dekel, A., & Silk, J. 1986, ApJ, 303, 39

Dolgov, A. D. 1980, Yadernaya Fizika (Sov. J. Nucl. Phys.), 31, 1522

Dolgov, A. D. 1999, hep-ph/9910532, Invited talk at Gamow's International Conference, St. Petersburg, August, 1999 (to be published in the Proceedings).

Dolgov, A.D. & Hansen, S.H. 2000, hep-ph/0009083.

Dolgov, A. D., Pastor, S., & Valle, J. W. F. 1995, FTUV/95-14, IFIV/95-14, (astro-ph/9506011)

Dolgov, A. D., Pastor, S., Romao, J. C., & and Valle, J. W. F Nucl.Phys. 1997, B 496, 24-40

Dubinski, J., & Carlberg, R. 1991, ApJ, 378, 496

Efstathiou, G. 1992, MNRAS, 256, P43

Eke, V. R., Cole, S., & Frenk, C. S. 1996, MNRAS, 282, 263

Eke, V. R., Efstathiou, G., & Wright, L. 1999, MNRAS, submitted (astro-ph/9908294)

Flynn, C., & Fuchs, B. 1994, MNRAS, 270, 471

Fall, S. M., & Efstathiou, G. 1980, MNRAS, 193, 189

Fukugita, M., Hogan, C. J., & Peebles, P. J. E. 1998, ApJ, 503, 518

Fukushige, T., & Makino, J. 1997, ApJ, 477, L9

Garriga, G. & Tanaka, T. 1999, hep-th/9911055

Gelato, S., & Sommer-Larsen, J. 1999, MNRAS, 303, 321

Gerstein, S.S. & Zeldovich, Ya. B. 1966, ZhETF Pis'ma Red. 4, 174

Giovanelli, R., et al. 1997, ApJ, 477, L1

Haardt, F., & Madau, P. 1996, ApJ, 461, 20

Haehnelt, M. G., Steinmetz, M. & Rauch, M. 1998, *ApJ*, 495, 647

Heavens, A., & Peacock, J. 1988, *MNRAS*, 232, 339

Hernquist, L., & Katz, N. 1989, *ApJS*, 70, 419

Hogan, C. J. 1999, *astro-ph/9912549*

Hogan, C. J., & Dalcanton, J. J. 2000, *astro-ph/0002330*

Huss, A., Jain, B., & Steinmetz, M. 1999, *ApJ*, 517, 64

Klypin, A., Kravtsov, A. V., Valenzuela, O., & Prada, F. 1999, *ApJ*, 523, 32

Kravtsov, A. V., Klypin, A. A., Bullock, J. S., & Primack, J. R. 1998, *ApJ*, 502, 48

van der Kruit, P. C., & Searle, L. 1982, *A&A*, 110, 61

de Laix, A. A., Scherrer, R. J., & Schaffer, R. K. 1995, *ApJ*, 452, 495

Mac Low, M.-M. & Ferrara, A. 1999, *ApJ*, 513, 142

Machacek, M. E. 1994, *ApJ*, 431, 41

Madau, P., et al. 1996, *MNRAS*, 283, 1388

Madsen, J. 2000, *astro-ph/0006074*

Malaney, R., Starkman, G., & Widrow, L. M. 1995, *Phys.Rev. D52*, 5480

McDonald, P., & Miralda-Escudé, J. 1999, *ApJ*, 519, 486

McDonald, P., et al. 1999, *ApJ*, submitted (*astro-ph/9911196*)

Mo, H. J., Mao, S., & White, S. D. M. 1998, *MNRAS*, 295, 319

Monaghan, J. J., & Gingold, R. A. 1983, *J. Comput. Phys.*, 52, 374

Moore, B., Governato, F., Quinn, T., Stadel, J., & Lake, G. 1998, *ApJ*, 499, L5

Moore, B., Ghinga, S., Governato, F., Lake, G., Quinn, T., Stadel, J., & Tozzi, P. 1999a, *ApJ*, 524, L19

Moore, B., Quinn, T., Governato, F., Stadel, J., & Lake, G. 1999b, *MNRAS*, submitted (*astro-ph/9903164*)

Navarro, J. F., & Benz, W. 1991, *ApJ*, 380, 320

Navarro, J. F., & White, S. D. M. 1994, MNRAS, 267, 401

Navarro, J. F., Frenk, C. S., & White, S. D. M. 1995, MNRAS, 275, 56

Navarro, J. F., Frenk, C. S., & White, S. D. M. 1996, ApJ, 462, 563

Navarro, J. F., & Steinmetz, M. 1997, ApJ, 478, 13

Navarro, J. F., & Steinmetz, M. 2000, ApJ, 528, 607

Nusser, A., & Haehnelt, M. 1999, MNRAS, submitted (astro-ph/9906406)

Pagels, H., & Primack, J. R. 1982, Phys. Rev. Lett., 48, 223

Peebles, P. J. E. 1980, The Large-Scale Structure of the Universe (Princeton: Princeton Univ. Press)

Peebles, P. J. E. 1993, Principles of Physical Cosmology (Princeton: Princeton Univ. Press)

Persic, M., & Salucci, P. 1992, MNRAS, 258, 14p

Persic, M., Salucci, P., & Stel, F. 1996, MNRAS, 281, 27

Pierpaoli, E., et al. 1998, Phys. Rev. D57, 2089

Primack, J. R. 1981, in Proceedings of the Banff Summer Institute on Particles and Fields, eds. A. Z. Capri and A. N. Kamal (New York: Plenum)

Primack, J. R., & Blumenthal, G. 1983, in Formation and Evolution of Galaxies and Large Structures in the Universe, eds. J. Audouze and J. Tran Thanh Van (Dordrecht: Reidel)

Quinn, T., Katz, N., & Efstathiou, G. 1996, MNRAS, 278, L41

Raffelt, G. 1996, Stars as Laboratories for Fundamental Physics (Chicago:University of Chicago Press)

Rohlfs, K., et al. 1986, A&A, 158, 181

Ryden, B. S., & Gunn, J. E. 1987, ApJ, 318, 15

Sackett, P. D. 1997, ApJ, 483, 103

Schaeffer, R., & Silk, J. 1988, ApJ, 332, 1

Sommer-Larsen, J. 1991, MNRAS, 250, 356

Sommer-Larsen, J., Gelato, S., & Vedel, H. 1999, ApJ, 519, 501 (SLGV99)

Spergel, D. N. & Steinhardt, P. J. 1999, astro-ph/9909386.

Steinmetz, M., & Navarro, J. F. 1999, ApJ, 513, 555

Steidel, C. C., et al. 1999, ApJ, 519, 1

Super-Kamiokande Collaboration 1998, Phys. Rev. Lett. 81, 1562

Syer, D., Mao, S., & Mo, H. J. 1997, MNRAS, submitted (astro-ph/9711160)

Thakar, A. R., & Ryden, B. S. 1998, ApJ, 506, 93

Vedel, H., Hellsten, U., & Sommer-Larsen, J. 1994, MNRAS, 271, 743

Weil, M. L., Eke, V. R., & Efstathiou, G. 1998, MNRAS, 300, 773

White, S. D. M., & Rees, M. J. 1978, MNRAS, 183, 341

White, S. D. M. 1993, in Les Houches Session LX, Cosmology and Large Scale Structure, ed. R. Schaeffer et al. (Amsterdam: Elsevier)

Yoshii, Y., & Arimoto, N. 1987, A&A, 188, 13

Zel'dovich, Ya. B. 1970, A&A, 5, 84

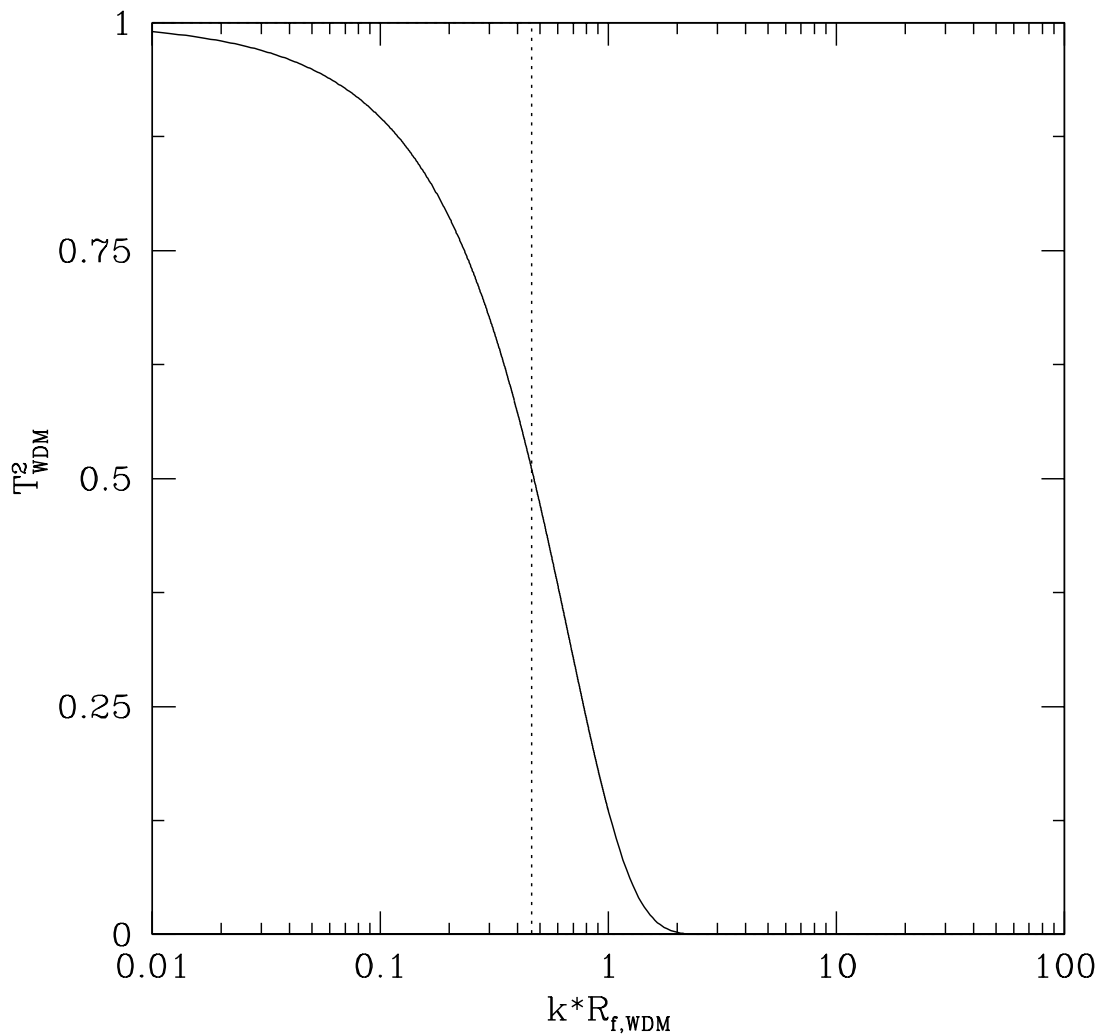


Fig. 1.— The square of the CDM to WDM transfer function (*solid line*) and the step-function approximation used in this work (*dotted line*).

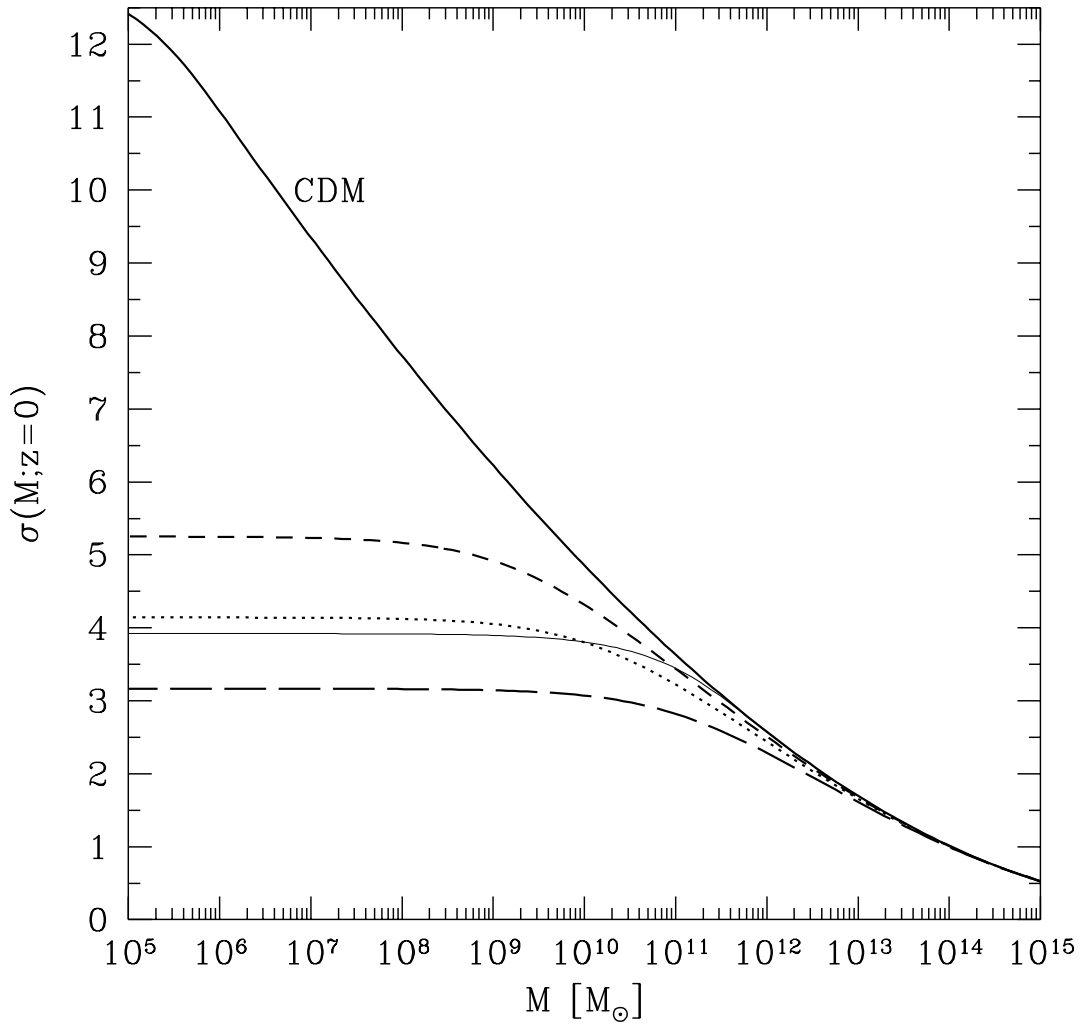


Fig. 2.— The mass fluctuation dispersion $\sigma(M)$ at $z=0$ for CDM (heavy solid line) and WDM with $M_{f, WDM} = 1.9 \times 10^{10} h^{-1} M_\odot$ (short-dashed line), $1.5 \times 10^{11} h^{-1} M_\odot$ (dotted line) and $1.2 \times 10^{12} h^{-1} M_\odot$ (long-dashed line). Also shown is $\tilde{\sigma}(M; z=0)$ for our step-function approximation to T_{WDM} for $M_{f, WDM} = 1.5 \times 10^{11} h^{-1} M_\odot$ (thin solid line).

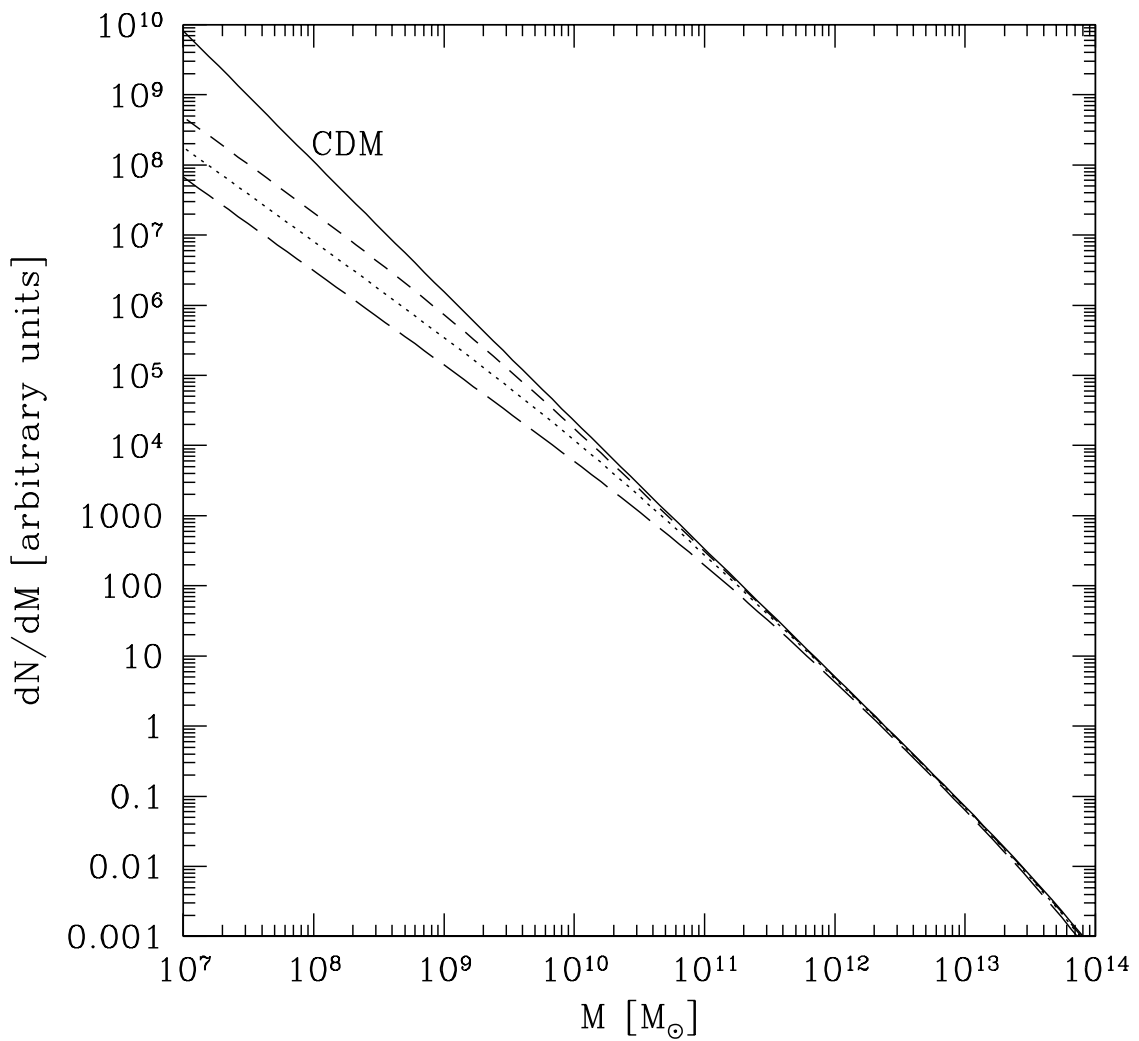


Fig. 3.— Mass spectra dN/dM at $z=0$ for CDM and the WDM from Fig. 2 (symbols as in Fig. 2).

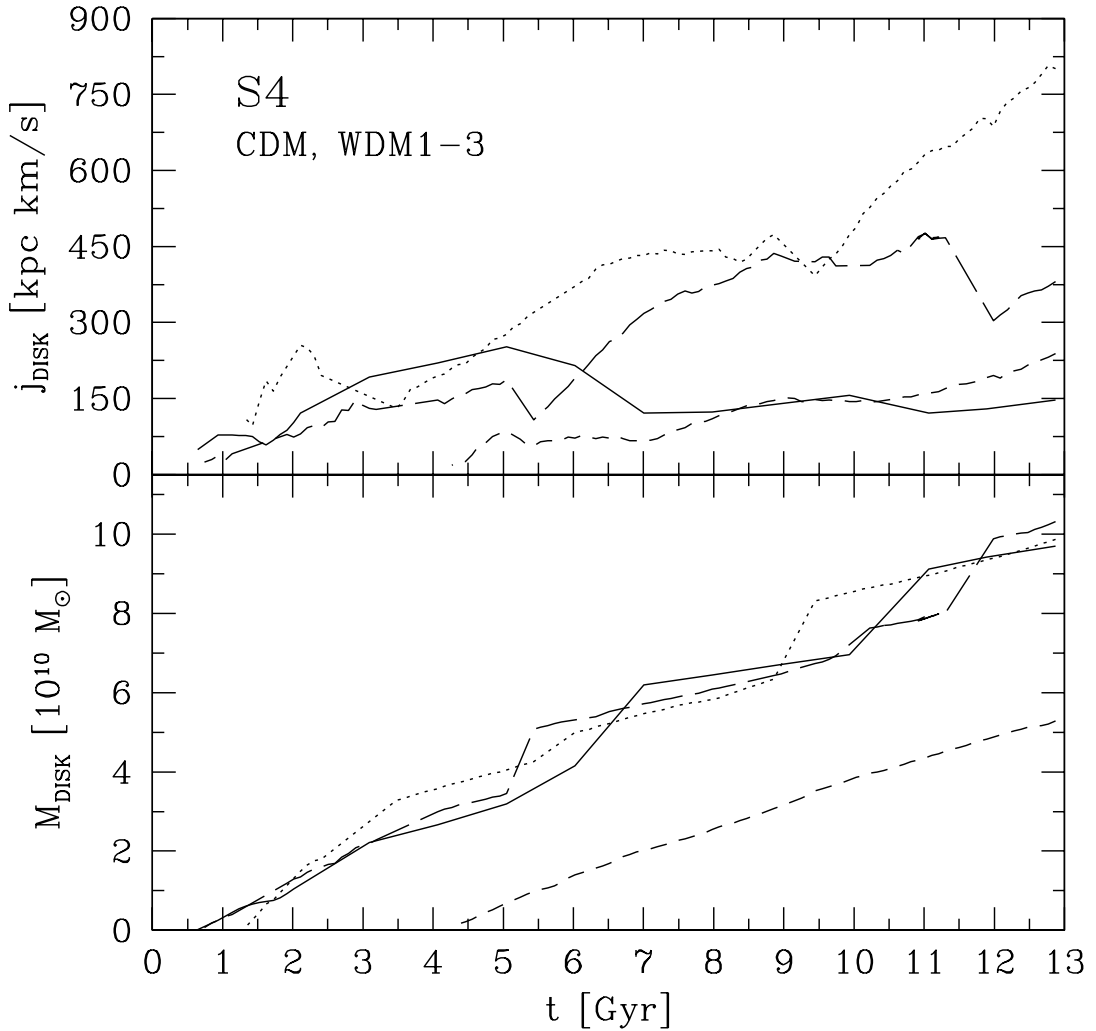


Fig. 4.— Specific angular momenta $j_{disk}(t)$ and cooled-out mass $M_{disk}(t)$ of the disk galaxies forming in the CDM and WDM1, WDM2, and WDM3, MR simulations (with $\Omega_b = 0.05$ and UVX radiation field) of galaxy S4 - symbols as in Fig. 2.

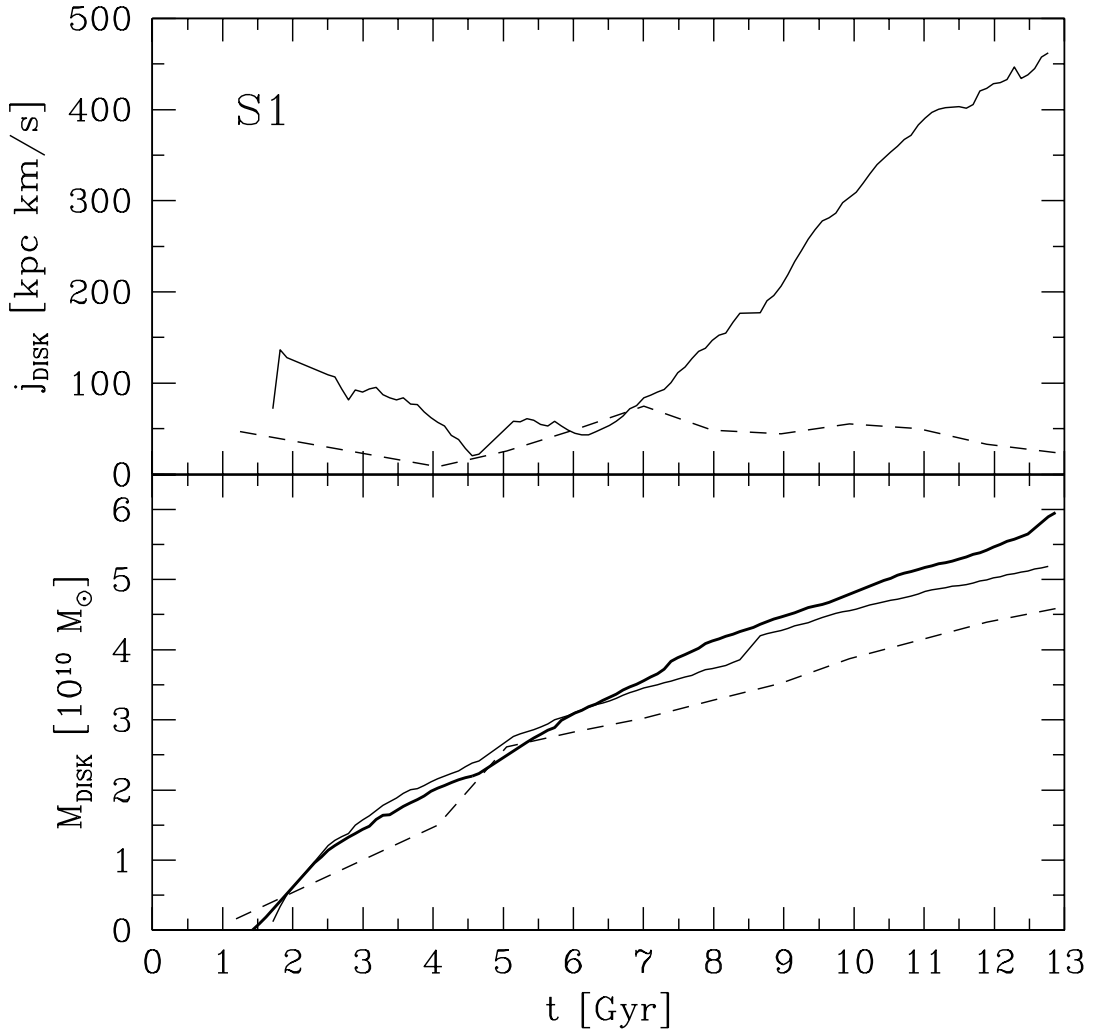


Fig. 5.— Specific angular momenta $j_{disk}(t)$ and cooled-out mass $M_{disk}(t)$ of the disk galaxies forming in the CDM (dashed lines) and WDM2, MR (solid lines) and HR (heavy solid lines) simulations (with $\Omega_b = 0.05$ and UVX radiation field) of galaxy S1 ($j_{disk}(t)$ is not shown for the HR simulation of this galaxy - see text).

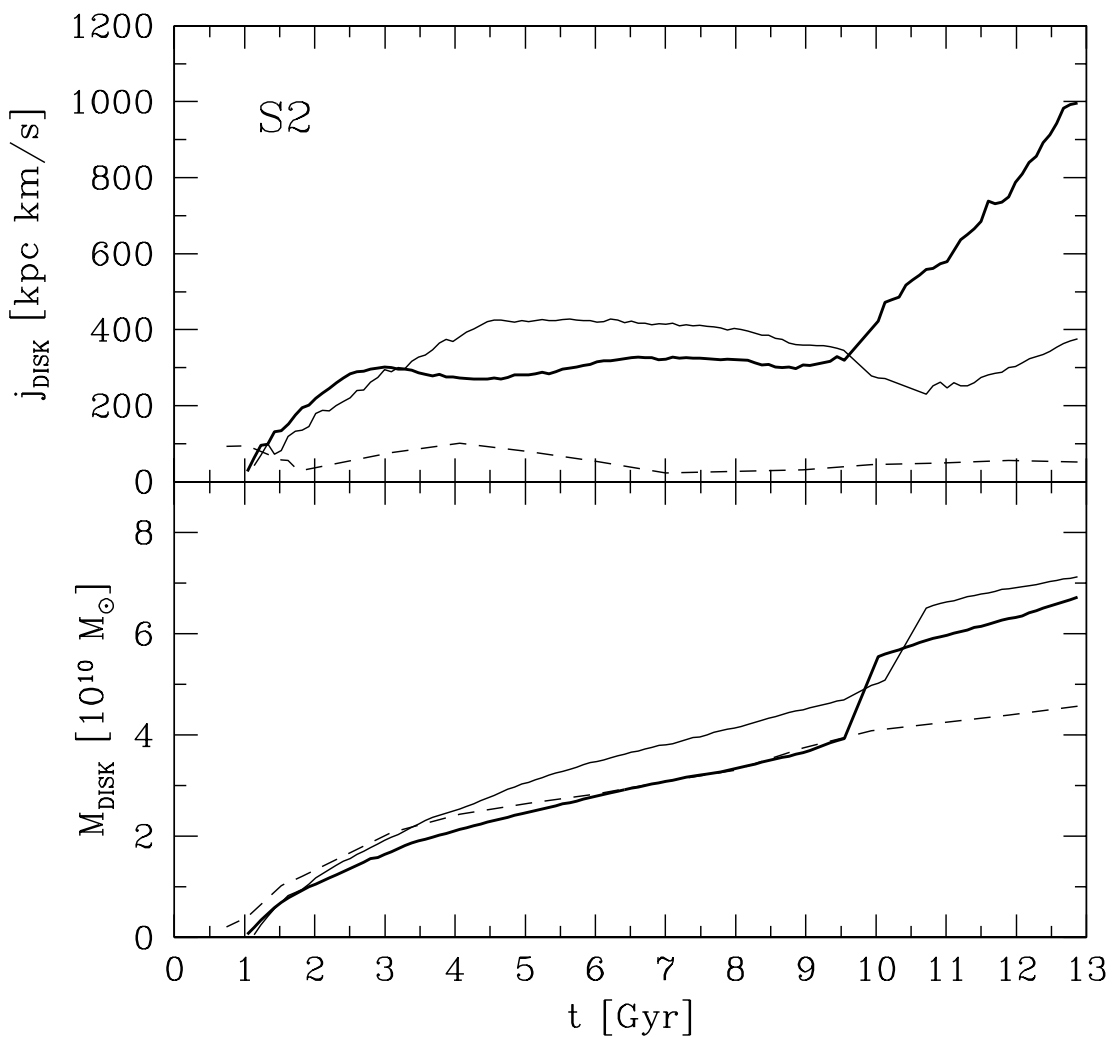


Fig. 6.— Same as in Fig. 5, but for galaxy S2.

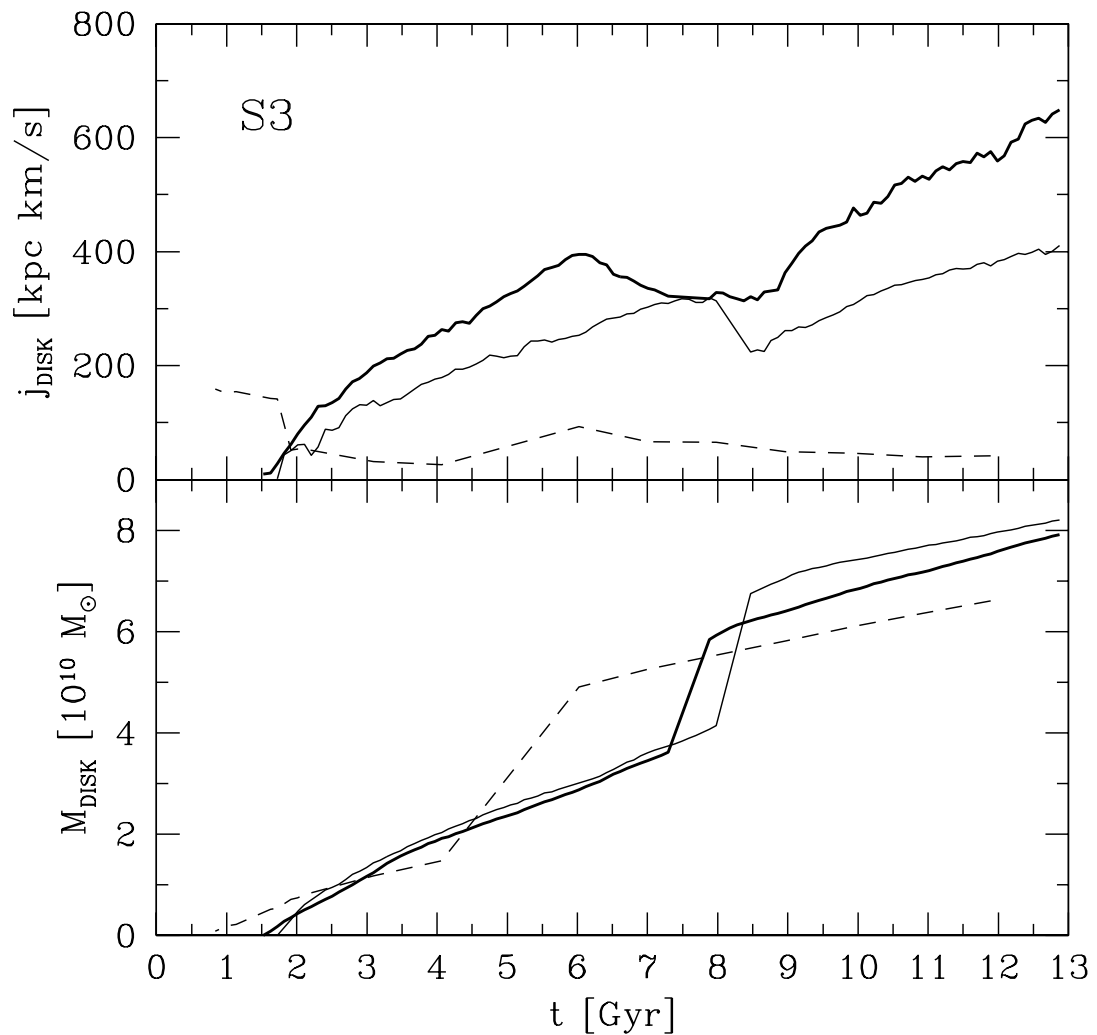


Fig. 7.— Same as in Fig. 5, but for galaxy S3.

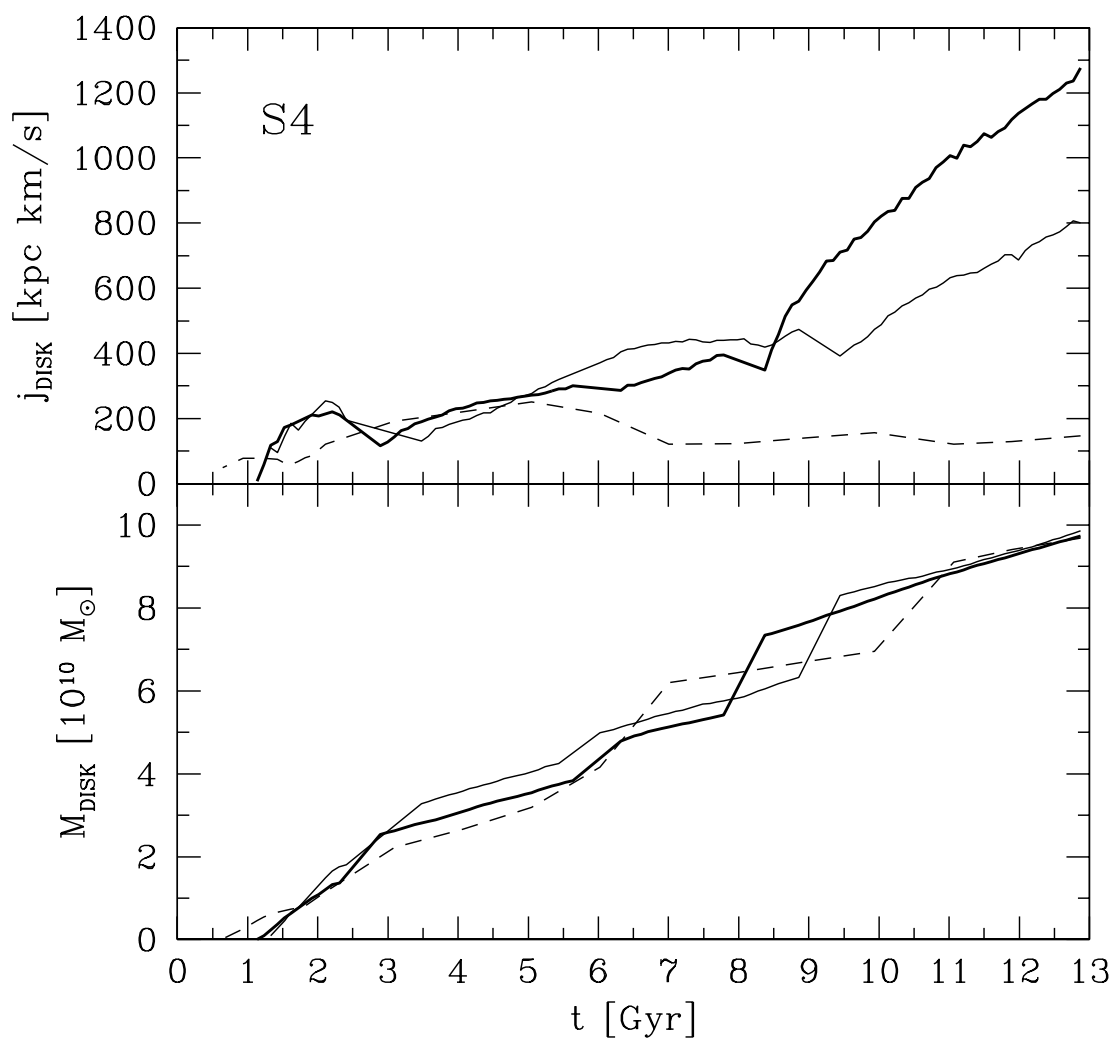


Fig. 8.— Same as in Fig. 5, but for galaxy S4.

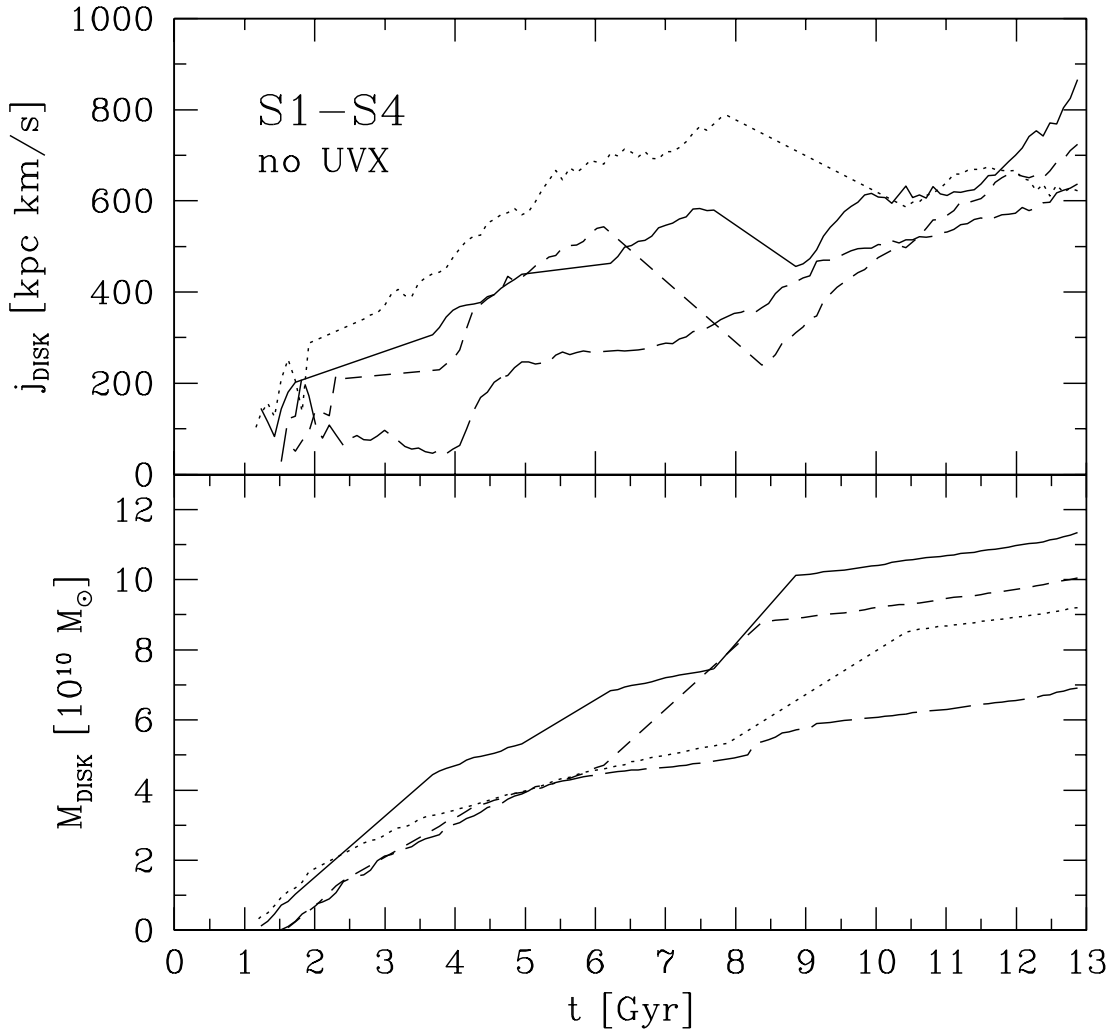


Fig. 9.— Specific angular momenta $j_{disk}(t)$ and cooled-out mass $M_{disk}(t)$ of the disk galaxies forming in the WDM2, MR simulations (with $\Omega_b = 0.05$ and no UVX radiation field) of galaxies S1 (long-dashed line), S2 (dotted line), S3 (short-dashed line) and S4 (solid line).

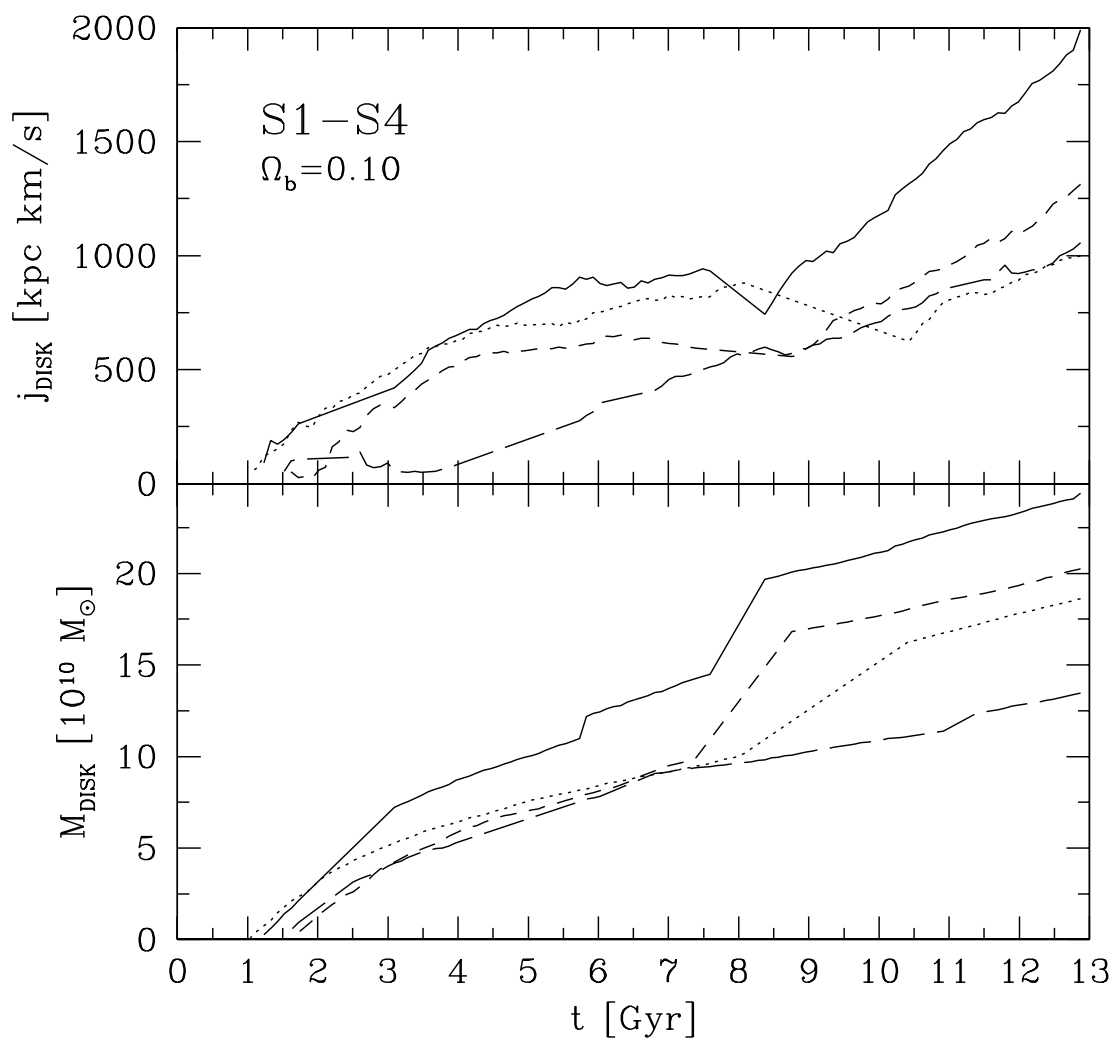


Fig. 10.— Same as in Fig. 9, but with $\Omega_b = 0.10$ and UVX radiation field.

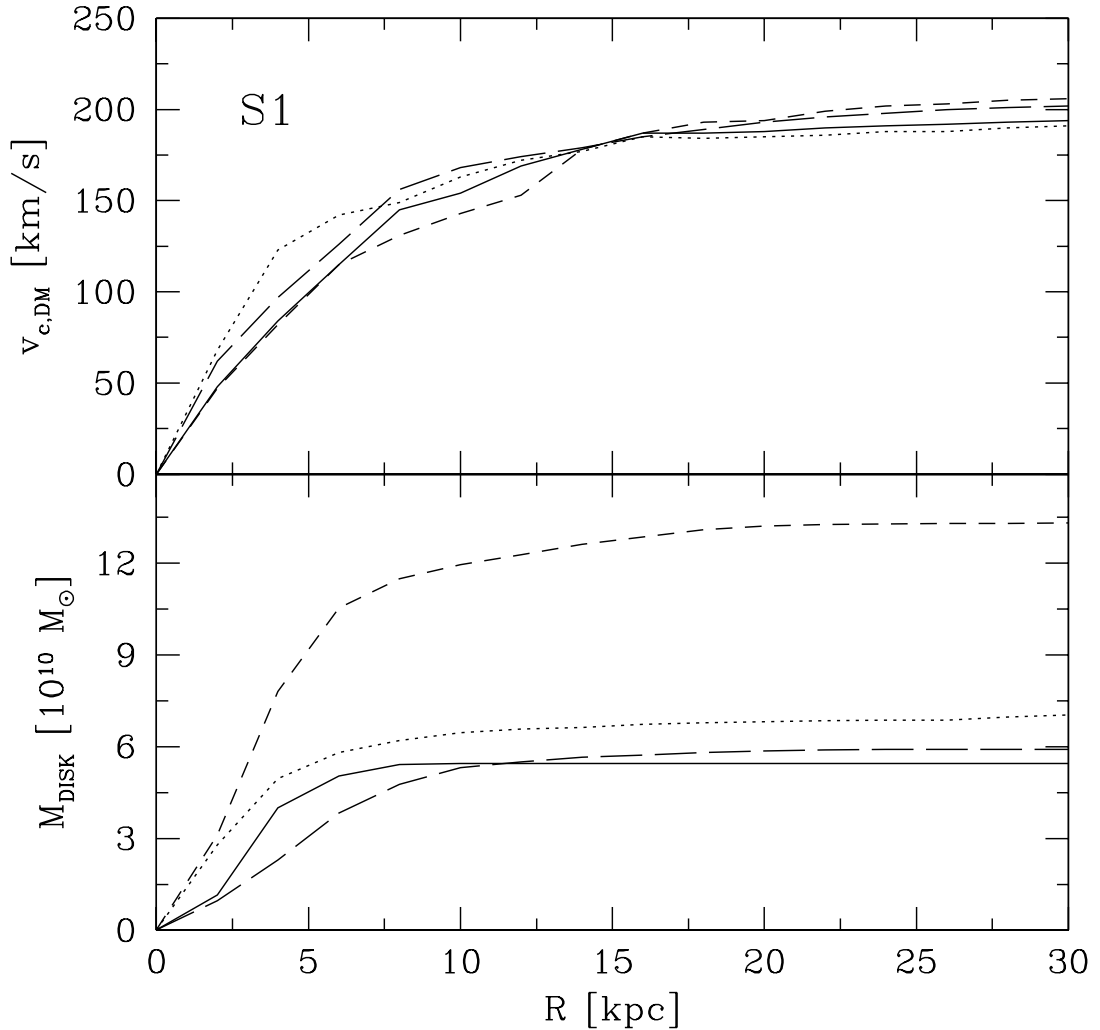


Fig. 11.— Circular velocity $v_{c,DM}(R)$ of the final dark matter halos and cooled-out disk mass $M_{disk}(R)$ of the final disk galaxies formed in the WDM2 simulations of galaxy S1: The MR run with $\Omega_b = 0.05$ and UVX radiation field (*solid lines*), the similar HR run (*long-dashed lines*), the MR run with $\Omega_b = 0.05$ and no UVX radiation field (*dotted line*) and the MR run with $\Omega_b = 0.10$ and UVX radiation field (*short-dashed lines*).

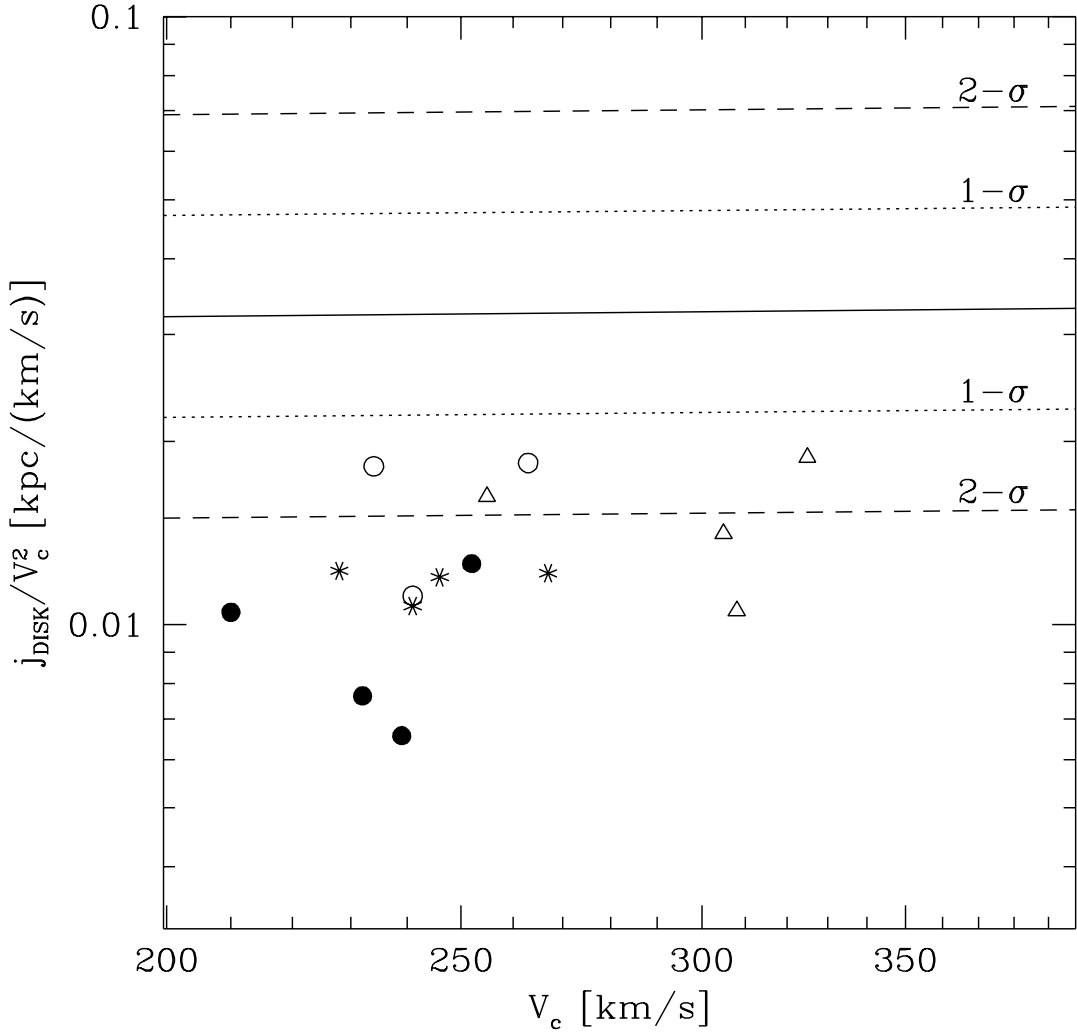


Fig. 12.— Normalized specific angular momenta $\tilde{j}_{\text{disk}} \equiv j_{\text{disk}}/V_c^2$ of the final disk galaxies formed in the WDM2 simulations: The MR runs with $\Omega_b = 0.05$ and UVX radiation field (*filled circles*), the similar HR run (*open circles*; S1 not shown - see text), the MR runs with $\Omega_b = 0.05$ and no UVX radiation field (*asterisks*) and the MR runs with $\Omega_b = 0.10$ and UVX radiation field (*open triangles*). The solid line shows the median value from the observational data, the dotted and dashed lines bracket the 1- σ and 2- σ intervals around this mean.

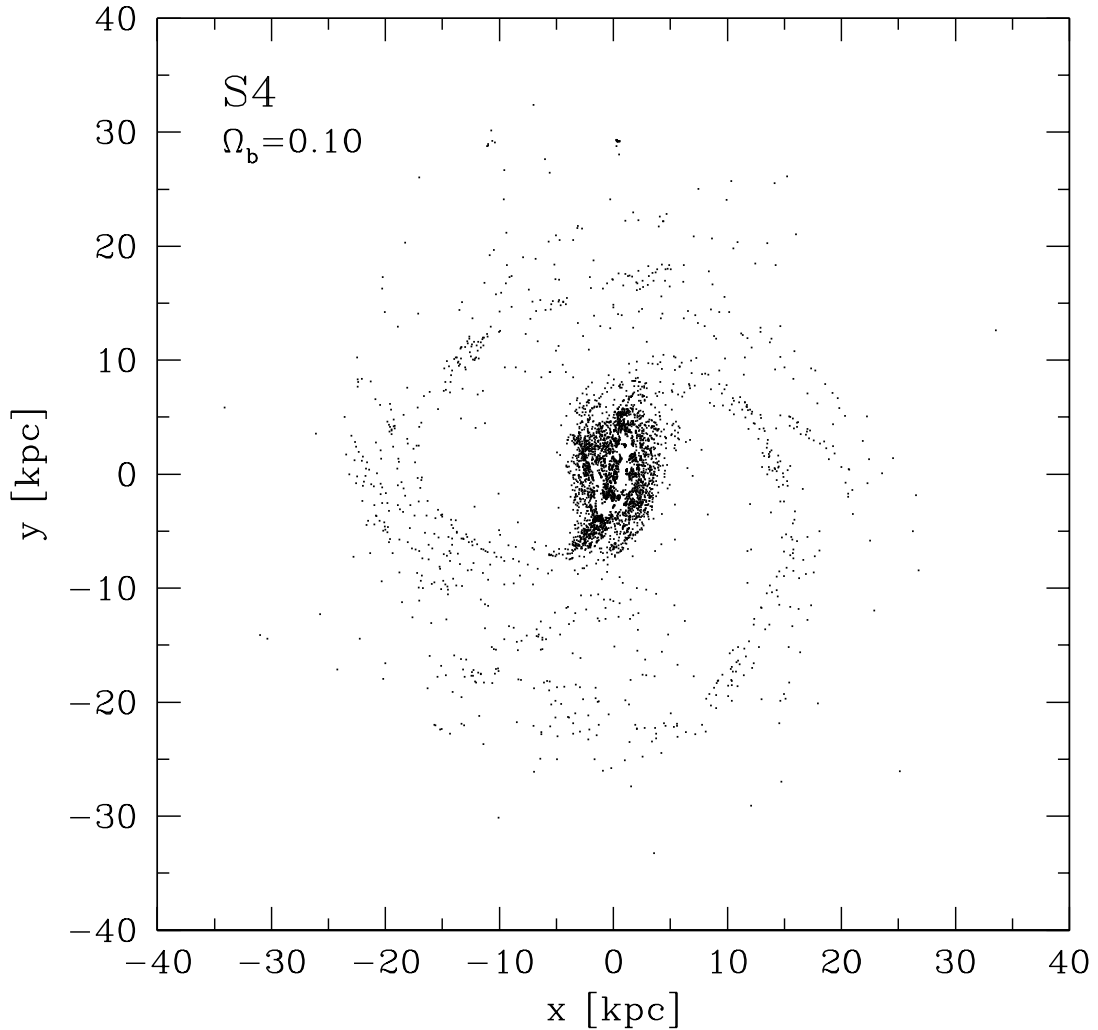


Fig. 13.— Face-on view of the final galaxy formed in run # 18 - this disk galaxy has the largest specific angular momentum of all galaxies formed in our WDM simulations, $j_{disk} \simeq 2000$ kpc km/s. Shown in the Figure are all ~ 4200 SPH particles in the central disk with $\log(T) < 4.5$.

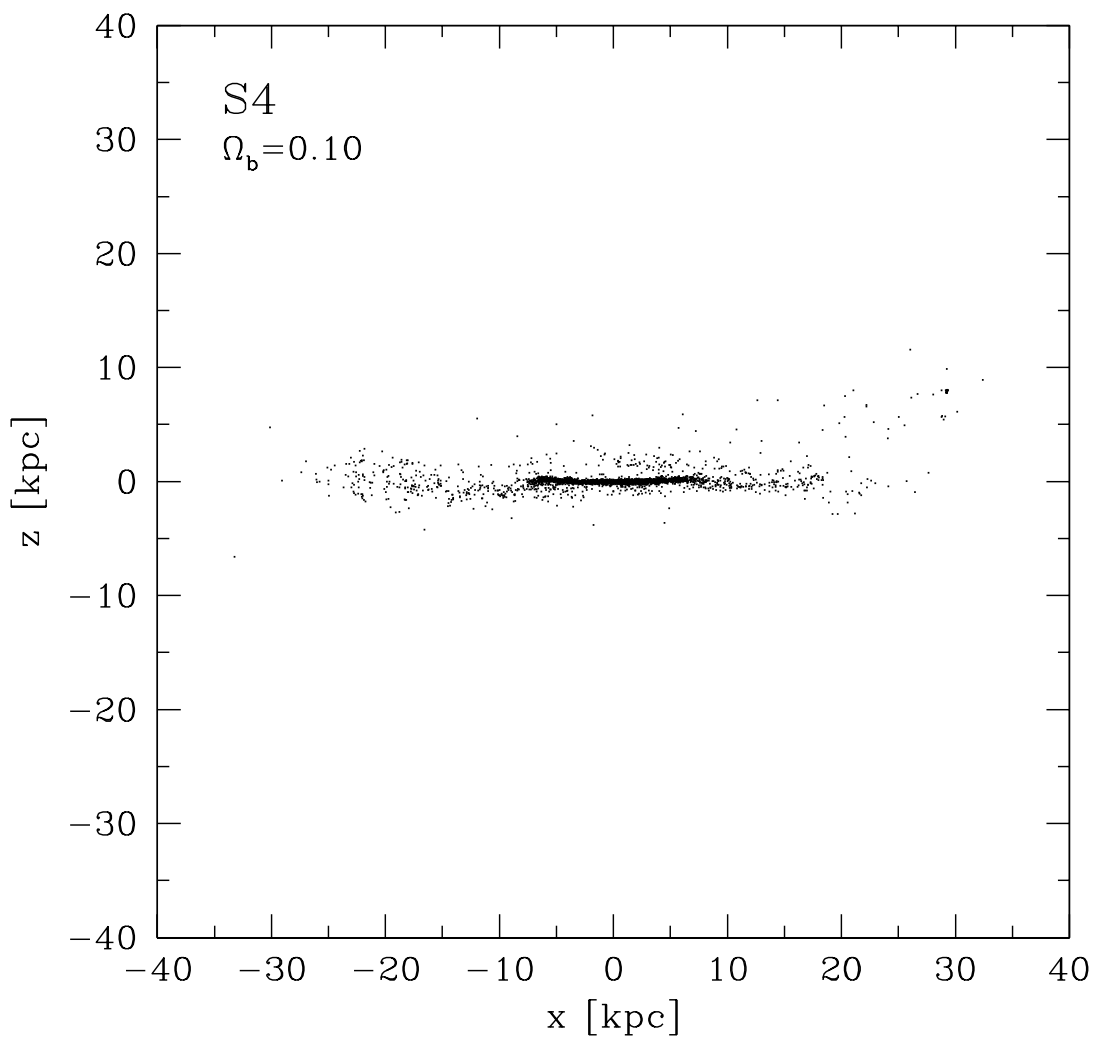


Fig. 14.— An edge-on view of the galaxy in Fig. 13.

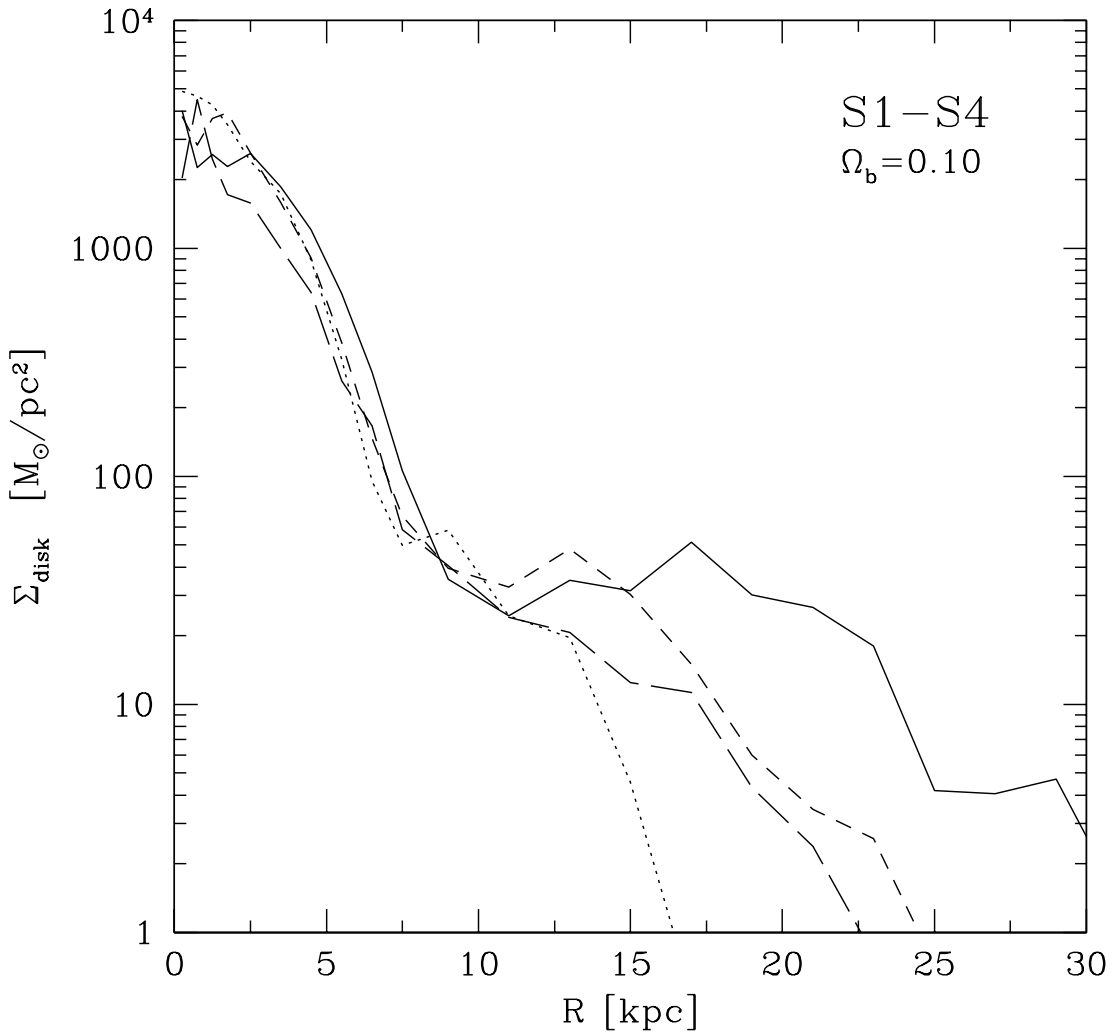


Fig. 15.—Azimuthally averaged disk surface density profiles of the final disk galaxies formed in the WDM2, MR simulations (with $\Omega_b = 0.10$ and UVX radiation field) of galaxies S1 (long-dashed line), S2 (dotted line), S3 (short-dashed line), and S4 (solid line).

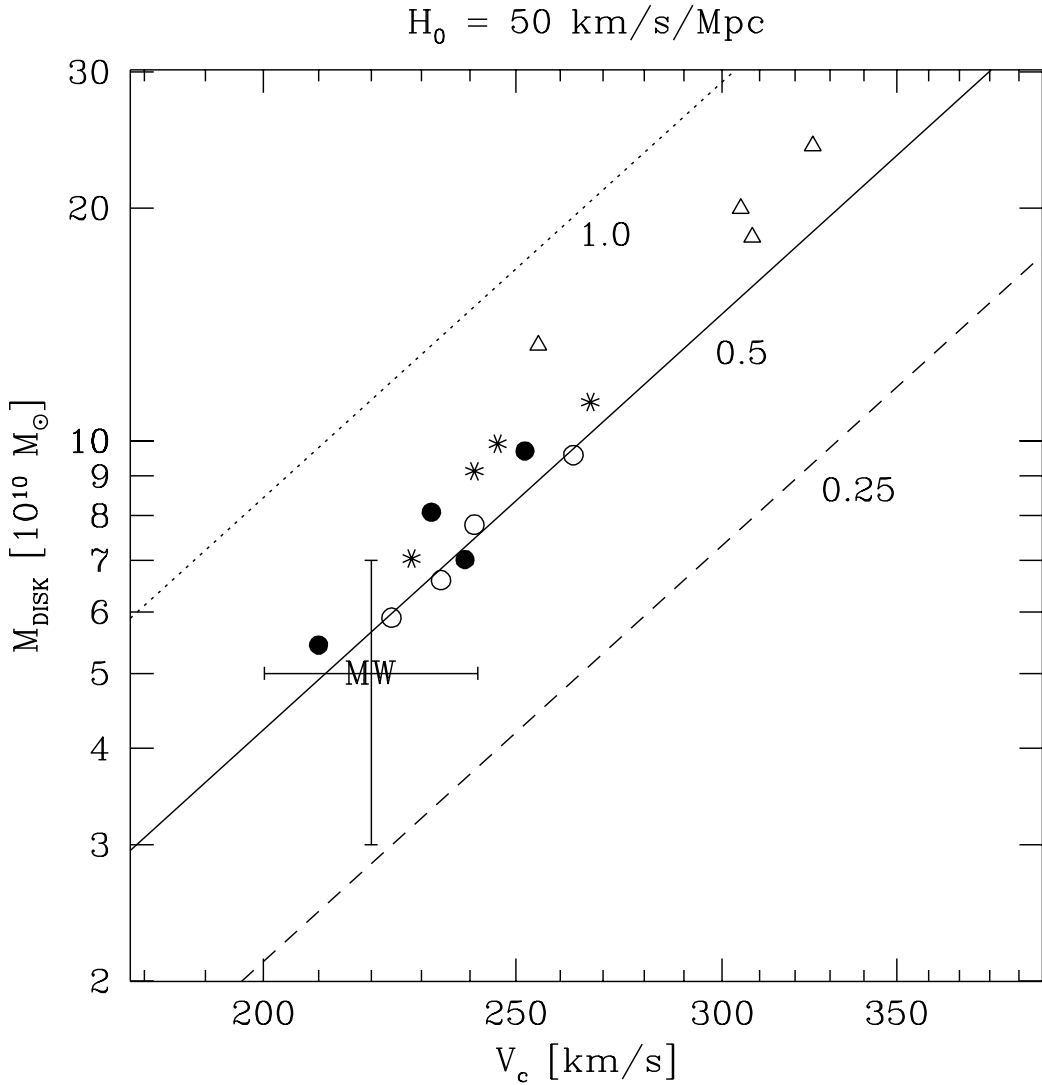


Fig. 16.— The mass vs. circular velocity “Tully-Fisher” relation for the final disks of our 16 WDM2 simulations - symbols used are the same as in Fig. 12. Also shown is the observed *I*-band TF relation of Giovanelli et al. converted to mass assuming $(M/L_I) = 0.25$ (*dashed line*), 0.5 (*solid line*) and 1.0 (*dotted line*). Finally, the symbol “MW” with errorbars shows the likely range of the total, baryonic mass and characteristic circular velocity of the Milky Way.

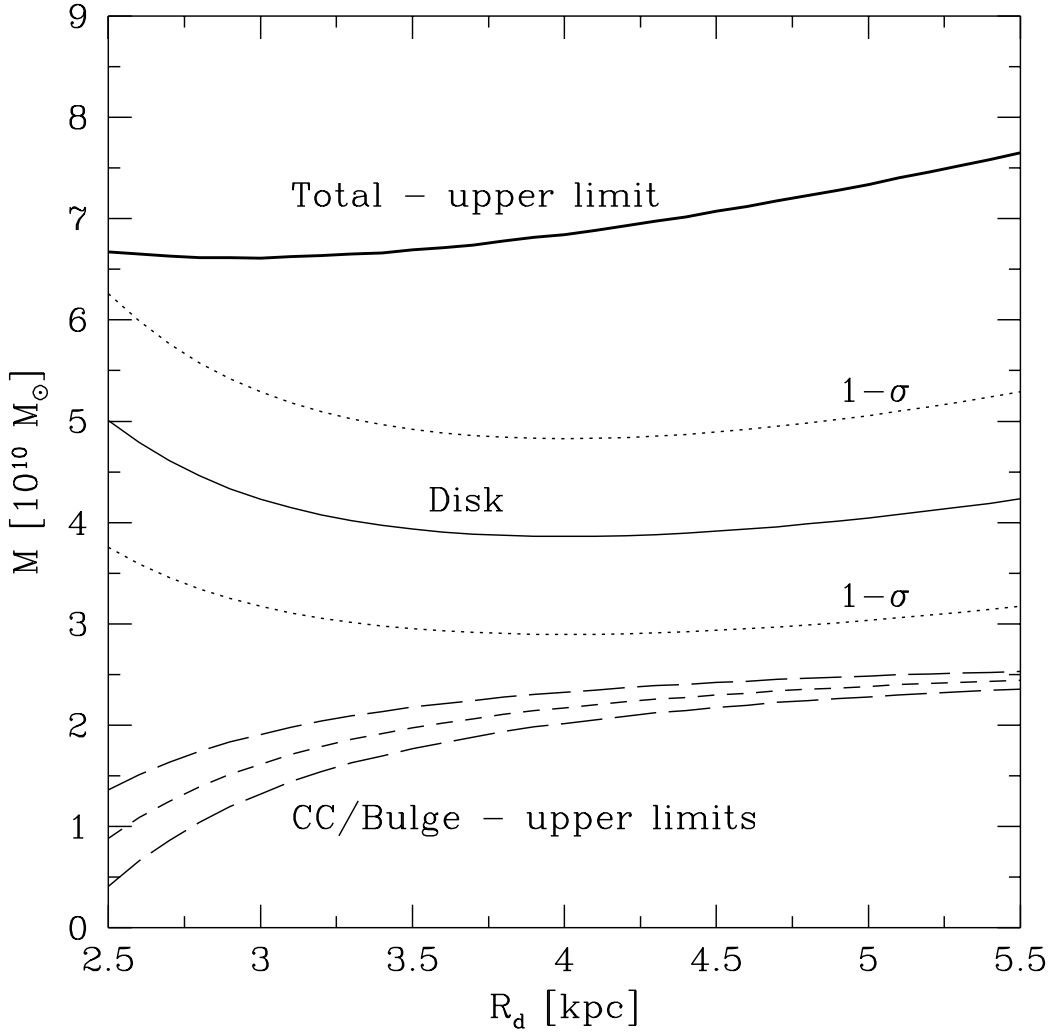


Fig. 17.— Baryonic mass of the Milky Way as a function of the disk scale-length R_d . The estimated mass of the disk is shown by the solid line and the $1-\sigma$ contours by the dotted lines. The upper limit to the mass of the central component/bulge is shown by the short-dashed line and lower and upper $1-\sigma$ contours by the long-dashed lines - see text for details. The $1-\sigma$ upper limit to the total, baryonic mass of the Milky Way is shown by the heavy, solid line.

Table 1: Parameters of the simulations

| Run | Galaxy | DM type | Resolution | UVX field | Ω_b | N_{SPH} | N_{DM} |
|-----|--------|---------|------------|-----------|------------|------------------|-----------------|
| 1 | S4 | WDM1 | MR | yes | 0.05 | 14736 | 7368 |
| 2 | S4 | WDM2 | MR | yes | 0.05 | 14700 | 7350 |
| 3 | S4 | WDM3 | MR | yes | 0.05 | 14848 | 7424 |
| 4 | S1 | WDM2 | MR | yes | 0.05 | 13700 | 6850 |
| 5 | S2 | WDM2 | MR | yes | 0.05 | 14142 | 7071 |
| 6 | S3 | WDM2 | MR | yes | 0.05 | 14404 | 7202 |
| 7 | S1 | WDM2 | HR | yes | 0.05 | 54689 | 54689 |
| 8 | S2 | WDM2 | HR | yes | 0.05 | 56386 | 56386 |
| 9 | S3 | WDM2 | HR | yes | 0.05 | 57723 | 57723 |
| 10 | S4 | WDM2 | HR | yes | 0.05 | 58739 | 58739 |
| 11 | S1 | WDM2 | MR | no | 0.05 | 13700 | 6850 |
| 12 | S2 | WDM2 | MR | no | 0.05 | 14142 | 7071 |
| 13 | S3 | WDM2 | MR | no | 0.05 | 14404 | 7202 |
| 14 | S4 | WDM2 | MR | no | 0.05 | 14700 | 7350 |
| 15 | S1 | WDM2 | MR | yes | 0.10 | 13700 | 6850 |
| 16 | S2 | WDM2 | MR | yes | 0.10 | 14142 | 7071 |
| 17 | S3 | WDM2 | MR | yes | 0.10 | 14404 | 7202 |
| 18 | S4 | WDM2 | MR | yes | 0.10 | 14700 | 7350 |

Table 2: Masses, sizes and velocities at $z = 0$

| Run | M_{200} [$10^{12} M_{\odot}$] | r_{200} [kpc] | V_{200} [km s $^{-1}$] | N_{gas} | N_{DM} | M_{gas} [$10^{10} M_{\odot}$] | M_{DM} [$10^{12} M_{\odot}$] | N_{disk} | M_{disk} [$10^{10} M_{\odot}$] | M_{disk} [$\Omega_b M_{200}$] |
|-----|--------------------------------------|--------------------|------------------------------|-----------|----------|--------------------------------------|-------------------------------------|------------|---------------------------------------|--------------------------------------|
| 1 | 3.25 | 382 | 191 | 5450 | 2850 | 15.59 | 3.10 | 3807 | 10.89 | 0.67 |
| 2 | 3.39 | 388 | 194 | 5663 | 2969 | 16.20 | 3.23 | 3392 | 9.70 | 0.57 |
| 3 | 2.42 | 346 | 173 | 4101 | 2098 | 11.82 | 2.30 | 1814 | 5.19 | 0.43 |
| 4 | 2.16 | 334 | 167 | 3590 | 1895 | 10.27 | 2.06 | 1903 | 5.44 | 0.50 |
| 5 | 2.37 | 344 | 172 | 4125 | 2074 | 11.80 | 2.25 | 2452 | 7.02 | 0.59 |
| 6 | 2.74 | 360 | 181 | 4812 | 2391 | 13.77 | 2.60 | 2824 | 8.08 | 0.59 |
| 7 | 2.18 | 334 | 167 | 15573 | 15206 | 11.14 | 2.07 | 8246 | 5.90 | 0.55 |
| 8 | 2.38 | 344 | 173 | 16955 | 16662 | 12.13 | 2.26 | 9224 | 6.60 | 0.55 |
| 9 | 2.68 | 358 | 179 | 19326 | 18686 | 13.82 | 2.54 | 10884 | 7.79 | 0.58 |
| 10 | 3.29 | 384 | 192 | 22602 | 23045 | 16.17 | 3.13 | 13392 | 9.70 | 0.58 |
| 11 | 2.15 | 332 | 167 | 3566 | 1822 | 10.20 | 2.05 | 2459 | 7.04 | 0.70 |
| 12 | 2.38 | 344 | 172 | 4429 | 2074 | 12.10 | 2.25 | 3191 | 9.13 | 0.77 |
| 13 | 2.78 | 362 | 182 | 4818 | 2426 | 13.78 | 2.64 | 3464 | 9.91 | 0.71 |
| 14 | 3.44 | 390 | 195 | 5801 | 3013 | 16.60 | 3.28 | 3922 | 11.22 | 0.66 |
| 15 | 2.16 | 332 | 167 | 3543 | 1892 | 20.27 | 1.95 | 2338 | 13.38 | 0.62 |
| 16 | 2.42 | 346 | 174 | 4357 | 2110 | 24.93 | 2.17 | 3203 | 18.33 | 0.76 |
| 17 | 2.83 | 364 | 183 | 4981 | 2475 | 28.50 | 2.55 | 3486 | 19.96 | 0.70 |
| 18 | 3.46 | 390 | 195 | 5945 | 3025 | 34.02 | 3.12 | 4205 | 24.06 | 0.69 |

Table 3: Circular velocities and specific angular momenta at $z = 0$

| Run | V_c [km s $^{-1}$] | λ | j_{disk} [kpc km s $^{-1}$] | r_{inf} [kpc] |
|-----|--------------------------|-----------|-----------------------------------|--------------------|
| 1 | 286 | 0.056 | 381 | 176 |
| 2 | 252 | 0.045 | 800 | 151 |
| 3 | 173 | 0.011 | 239 | 120 |
| 4 | 210 | 0.026 | 462 | 122 |
| 5 | 239 | 0.027 | 375 | 145 |
| 6 | 232 | 0.045 | 411 | 149 |
| 7 | 224 | 0.017 | - | 132 |
| 8 | 234 | 0.025 | 997 | 134 |
| 9 | 241 | 0.049 | 648 | 144 |
| 10 | 263 | 0.050 | 1276 | 150 |
| 11 | 228 | 0.018 | 637 | 166 |
| 12 | 241 | 0.018 | 623 | 199 |
| 13 | 246 | 0.046 | 724 | 201 |
| 14 | 267 | 0.052 | 866 | 178 |
| 15 | 255 | 0.020 | 1056 | 148 |
| 16 | 308 | 0.022 | 1000 | 201 |
| 17 | 305 | 0.045 | 1312 | 194 |
| 18 | 325 | 0.054 | 1990 | 186 |